Karlsruher Institut für Technologie
Institut für Baustatik

Dielectric Elastomers - Numerical Modeling of Nonlinear Visco-Electroelasticity

A. Büschel, S. Klinkel, W. Wagner

Mitteilung 4(2012)

Karlsruher Institut für Technologie
Institut für Baustatik

Dielectric Elastomers - Numerical Modeling of Nonlinear Visco-Electroelasticity

A. Büschel, S. Klinkel, W. Wagner

Mitteilung 4(2012)

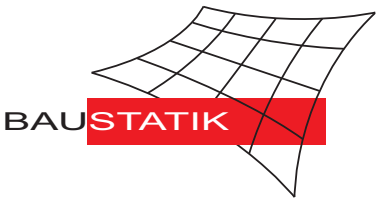

Prof. Dr.–Ing. W. Wagner
Institut für Baustatik
Karlsruher Institut für Technologie
Kaiserstr. 12
76131 Karlsruhe

Telefon: +49 721 608 42280
Telefax: +49 721 608 46015
E–mail: info@ibs.kit.edu
Internet: http://www.ibs.kit.edu

Dielectric elastomers – Numerical modeling of nonlinear visco-electroelasticity

A. Büschel[1], S. Klinkel[2], W. Wagner[1]

[1]Institute for Structural Analysis, Karlsruhe Institute of Technology (KIT), Kaiserstr. 12, 76131 Karlsruhe, Germany
[2]Chair of Structural Mechanics, RWTH Aachen University, Mies-van-der-Rohe-Str. 1, 52074 Aachen, Germany

Contents

Abstract

Dielectric elastomer actuators, which can directly turn electrical energy into mechanical energy belong to the group of electroactive polymers (EAP). This type of electroelastic material exhibits large displacement characteristics, and is able to change its mechanical behavior in response to the application of an electric field. Dielectric actuators are made out of elastomers which in general show viscoelastic behavior. To take this time dependent effect into account, the deformation gradient is multiplicatively decomposed. The paper is focused on the numerical modeling of soft dielectric elastomers. The theoretical foundation and the consistent finite element implementation is outlined based on the laws of electricity and elasticity. Furthermore, numerical examples of the nonlinear visco-electroelasticity model are shown.

1 Introduction

In recent decades, great efforts have been directed towards the development of active and multifunctional materials. These materials have the potential to transform passive structures into adaptive systems. An overview is given in [1, 2, 3]. However, a prerequisite for the design and the optimization of these materials is that reliable models exist, which incorporate physical processes.
Polymeric electroelastic materials, or electroactive polymers, have the following characteristic: they deform by the application of an electric field. The benefit of EAPs is that they share the characteristics of polymers; they are lightweight, inexpensive in production, fracture tolerant and elastic. Furthermore, the physical and chemical structure is well understood. Due to the similarities with biological tissues in terms of achievable stresses and forces, they are often called artificial muscles. Products will gain new dimensions ranging from changing tactile surfaces over active membranes to morphing shapes.
The designation electroactive polymer is a generic term for different active polymeric materials. A good overview can be found in [8, 9, 10, 11]. Based on their mechanism to deform, EAP‘s can be divided into two major categories: electronic/electric or field activated and ionic activated EAP‘s. Also referred to as dry and wet EAP’s. De novo, Electric EAP’s are subdivided into electrostrictive polymers, ferroelectric polymers, polymer electrets, and dielectric elastomers [4, 6]. The deformation originates due to two electromechanical stresses, the Maxwell stress and the electrostriction. The Maxwell stress emerge due to electrostatic force between electric charges. This force is discussed in Coulombs law. A brief recapitulation is given in section 2. The influence of the electristriction goes back to the intramolecular forces. The stress caused by electristriction is small against the Maxwell stress [5]. In contrast to electronic EAP‘s, the ionic EAP’s are driven by diffusions and intermolecular movements of ions. They consist of two electrodes, an electrolyte and the activatable material. One of their advantages is the use of a low activation voltage ($1-2\,V/\mu m$), instead of high activation voltage by dry EAP’s (in orders of $10-100\,V/\mu m$).
The focus in this paper is on the numerical modeling of the dielectric elastomers (DE). Soft dielectric elastomers have the character to be able to produce large strains while sustaining moderate forces by applying an electric field. The principle setup of DE’s is a soft dielectric material arranged between elastic, conductive electrodes. The electrodes have to be highly compliant to ensure that they don‘t impede the deformation. In the past the influence of the Maxwell stress was treated as a perturbing effect, because of the nearly neglecting induced stresses. Owing to the consistent development of polymers this point of view has changed, through the development of polymers with lower elasticity and higher dielectric strength. Now it is possible to realize actuator applications. DE’s can also be used as sensors. By applying a force or a displacement, an electric field will be produced. As it is mentioned above the electronic polymers require a high electric field for activation. To deal with moderate fields, the dielectric elastomer actuator thickness have to be film-like. Another option to reduce the high activation fields is to use polymers with high dielectric constants. This can be performed by filling polymers with highly dielectric components for example ceramics. Several possible actuators/sensors configurations have been developed; tube, roll, helical, bi-, unimorph bender, stapled, folded, diaphragm and planar. All of them use the fact, that the film is squeezed in the direction of the electric field. This causes expansion in the transverse planar direction because of the nearly incompressibility character of the elastomer. Section 2.1 and 2.2 introduce the basic mechanical- and electrodynamic equations. As mentioned above a brief recapitulation of the acting forces is given at the end of this subsections. Details can be found for example in [12, 26, 27]. The next subsections bring the two theories together with the assistance of the Maxwell stress and the coupling in the free energy function, see also [28, 29, 30, 31, 23, 24, 32]. In sec-

tion 3 the fundamental equations are repeated. Furthermore the formulation for the finite element implementation is prepared based on a variational approach [25]. To incorporate viscoelasticity, the deformation gradient is multiplicatively decomposed into an elastic and an inelastic (viscous) part. This is based on the concept published by [13, 14, 15, 16]. The free energy function is additively decomposed into an elastic and inelastic part. The elastic and inelastic part is derived from a potential which is reasonable for rubber-like materials [17]. Other approaches can be found in [18, 19, 20, 36, 37]. The solution strategy of the multiplicative split is summarized in subsection 3.3. In all its elaborateness it is pointed out in the preceding references. In section 2 and 3 the theoretical background is presented in detail. In section 4 numerical examples are given. In this section a free energy function is used which was first introduced in [12, 28]. In the first example a spherical shell is considered. To validate the numerical model without viscous effects a solution is found for two different boundary conditions with MAPLE$^{\text{TM}}$[1][38] and compared with the numerical model. A plate with a hole under electrical loading for several relaxation times is discussed in the second example. Finally a coiled actuator under the influence of a sinusoidal loading with various frequencies is demonstrated. The paper is concluded with a summary and an outlook.

2 Basic equations

2.1 Kinematics

Let us consider a deformable electrically sensitive body with its reference configuration $\mathcal{B}_0$ in the absence of electric fields and mechanical loads. This is known as stress-free configuration. The region in three-dimensional Euclidean space of $\mathbb{R}^3$ is occupied by the body. The boundary of $\mathcal{B}_0$ is denoted by $\partial\mathcal{B}_0$. The position vector of a particle within this body in the reference configuration is given by $\vec{\boldsymbol{X}}$. In the deformed configuration, the position of the particle is denoted by $\vec{\boldsymbol{x}} = \vec{\boldsymbol{\chi}}(\vec{\boldsymbol{X}})$ and this particle occupies the current configuration $\mathcal{B}_t$. $\vec{\boldsymbol{\chi}}$ is a one to one, twice continuously differentiable mapping. The boundary of $\mathcal{B}_t$ is referred to as $\partial\mathcal{B}_t$. In this paper lower case operator symbols and letters for formula symbols generally operate with respect to the current configuration. Upper case operator symbols and letters for formula symbols generally operate in accordance with the reference configuration. Vectors are denoted bold-faced with an arrow above the letter. Second order tensors are denoted bold type. For higher order tensors, blackboard bold typeface is used. The deformation gradient

$$\boldsymbol{F} = \mathrm{Grad}\,(\vec{\boldsymbol{\chi}}) \quad \text{with} \quad J = \det(\boldsymbol{F}), \tag{1}$$

consisting of the gradient with respect to the reference configuration, describes the change of movement within the close surrounding of the material particle $\vec{\boldsymbol{X}}$. For its determinant J one has $J > 0$. It shall use the notation $\boldsymbol{F}^{-T} = (\boldsymbol{F}^{-1})^T$. The gradient operator of a vector field is acting at the current configuration which is given as $\mathrm{grad}(\dots) = \frac{\partial(\dots)_i}{\partial \vec{\boldsymbol{x}}_j}\vec{\boldsymbol{i}}_i \otimes \vec{\boldsymbol{i}}_j$, and is defined as $\mathrm{Grad}(\dots) = \frac{\partial(\dots)_i}{\partial \vec{\boldsymbol{X}}_j}\vec{\boldsymbol{i}}_i \otimes \vec{\boldsymbol{i}}_j$ with respect to the reference configuration. In this contribution the symbol $\otimes$ stands for the tensor product and the Einstein summation convention over repeated indices is used. For the base vectors, cartesian coordinates are used and $\vec{\boldsymbol{i}}_i \cdot \vec{\boldsymbol{i}}_j = \boldsymbol{\delta}_{ij}$. Whereby $\boldsymbol{\delta}_{ij}$ is the Kronecker delta, which is one for repeated indices and otherwise zero. The dot represents the inner product. The right and left

[1] Maple is a trademark of Waterloo Maple Inc.

Cauchy-Green symmetric deformation tensors are associated with $\boldsymbol{F}$ and defined by

$$\boldsymbol{C} = \boldsymbol{F}^T\boldsymbol{F} = \sum_{A=1}^{3} \lambda_A^2\, \vec{\boldsymbol{N}}_A \otimes \vec{\boldsymbol{N}}_A \quad \text{and} \quad \boldsymbol{b} = \boldsymbol{F}\boldsymbol{F}^T = \sum_{A=1}^{3} \lambda_A^2\, \vec{\boldsymbol{n}}_A \otimes \vec{\boldsymbol{n}}_A, \tag{2}$$

respectively. It holds $\det(\boldsymbol{b}) = \det(\boldsymbol{C}) = J^2$. In addition, the principal stretches λ_A, $A = 1, 2, 3$ are related to the determinant of $\boldsymbol{F}$ based on $J = \lambda_1\lambda_2\lambda_3$. The orthonormal vectors, characterized by $\vec{\boldsymbol{n}}_A$ and $\vec{\boldsymbol{N}}_A$, denote the direction of the stretch in the current and reference configuration, respectively.
The spatial total time derivative is given by $\frac{\partial}{\partial t}\chi(\vec{\boldsymbol{x}}, t)|_{\vec{\boldsymbol{x}}-fixed}$ and the material derivation to $\frac{\partial}{\partial t}\chi(\chi^{-1}(\vec{\boldsymbol{X}}, t), t)|_{\vec{\boldsymbol{X}}-fixed}$, respectively. The material velocity gradient is given as

$$\dot{\boldsymbol{F}} = \mathrm{Grad}(\dot{\vec{\boldsymbol{x}}}), \quad \text{and} \quad \boldsymbol{l} = \dot{\boldsymbol{F}}\boldsymbol{F}^{-1} = \mathrm{grad}(\dot{\vec{\boldsymbol{x}}}) \tag{3}$$

denotes the spatial velocity gradient. Where $(\dot{\therefore})$ designated the material time derivative. In consideration of viscoelasticity, the "total" deformation gradient $\boldsymbol{F}$ is multiplicatively decomposed into an elastic part $\boldsymbol{F}_e$ and a viscous part $\boldsymbol{F}_v$,

$$\boldsymbol{F} = \boldsymbol{F}_e\boldsymbol{F}_v. \tag{4}$$

This split can be interpreted in case of a theory of small deformations as an additive split of the strain $\boldsymbol{\varepsilon} = \boldsymbol{\varepsilon}_e + \boldsymbol{\varepsilon}_v$ and can be compared with a rheological model which consist of a spring parallel-connected with a stated number of Maxwell elements. The elastic right and left Cauchy-Green tensor are expressed as follows

$$\boldsymbol{C}_e = \boldsymbol{F}_v^{-T}\boldsymbol{C}\boldsymbol{F}_v^{-1} \quad \text{and} \quad \boldsymbol{b}_e = \boldsymbol{F}\boldsymbol{C}_v^{-1}\boldsymbol{F}^T. \tag{5}$$

Elastomers behave nearly incompressible. Hence, for the numerical modeling it is common to decompose multiplicative the deformations gradient into a volumetric $\boldsymbol{F}_{vol} = J^{1/3}\boldsymbol{I}$ and an isochoric part $\boldsymbol{F}_{iso} = \tilde{\boldsymbol{F}}$, with $\det[\tilde{\boldsymbol{F}}] = \det[\tilde{\lambda}_1\tilde{\lambda}_2\tilde{\lambda}_3] = 1$. Herein, $\boldsymbol{I} = \delta_{ij}\,\vec{\mathbf{i}}_i \otimes \vec{\mathbf{i}}_j$ denotes the second order identity tensor and $\tilde{\lambda}_A = J^{-1/3}\lambda_A$, $A = 1, 2, 3$ characterize the purely isochoric principal stretches. In the course of this contribution the following definitions for the isochoric $\tilde{\boldsymbol{C}}$ and the isochoric elastic right Cauchy-Green tensor $\tilde{\boldsymbol{C}}_e$ are needed

$$\tilde{\boldsymbol{C}} = J^{-\frac{2}{3}}\boldsymbol{C} = \sum_{A=1}^{3} \tilde{\lambda}_A^2\, \vec{\boldsymbol{N}}_A \otimes \vec{\boldsymbol{N}}_A \quad \text{and} \quad \tilde{\boldsymbol{C}}_e = J_e^{-\frac{2}{3}}\boldsymbol{C}_e = \sum_{A=1}^{3} \tilde{\lambda}_{Ae}^2\, \vec{\boldsymbol{N}}_A \otimes \vec{\boldsymbol{N}}_A. \tag{6}$$

Here, $J_e = \lambda_{1e}\lambda_{2e}\lambda_{3e}$ describes the determinant of $\boldsymbol{F}_e$ and $\tilde{\lambda}_{Ae}$, $A = 1, 2, 3$ are the principal values of $\tilde{\boldsymbol{C}}_e = \tilde{\boldsymbol{F}}_e^T\tilde{\boldsymbol{F}}_e = J_e^{-2/3}\boldsymbol{F}_e^T\boldsymbol{F}_e$.

2.2 Electrostatic Equations

The four Maxwell equations describe the behavior of electric and magnetic fields. These relations cover interactions with matter, too [12]. This contribution discuss dielectrics which can be polarized by an applied electric field. Assuming that the considered material owns no free charges ρ_f, shows no response to magnetic fields or magnetic induction and considering a quasistatic process, the Maxwell equations can be reduced to:

$$\mathrm{curl}(\vec{\boldsymbol{e}}) = \vec{\mathbf{0}} \quad \text{and} \quad \mathrm{div}(\vec{\boldsymbol{d}}) = 0 \tag{7}$$

In addition the rotation-operator is defined as $\operatorname{curl}(\dots) = \varepsilon_{ijk}\frac{\partial(\dots)_j}{\partial\vec{\boldsymbol{x}}_i}\vec{\boldsymbol{i}}_k$ and the divergence-operator of a vector field is hereby assigned with $\operatorname{div}(\dots) = \frac{\partial(\dots)_i}{\partial\vec{\boldsymbol{x}}_i}$. Where $\boldsymbol{\mathcal{E}} = \varepsilon_{ijk}\vec{\boldsymbol{i}}_i \otimes \vec{\boldsymbol{i}}_j \otimes \vec{\boldsymbol{i}}_k$ is the third-order permutation tensor.
The fields $\vec{\boldsymbol{e}}$ and $\vec{\boldsymbol{d}}$ are the electric field and the electric displacement field, respectively. These are Eulerian vector fields. The Lagrangian versions are defined by

$$\operatorname{Curl}(\vec{\boldsymbol{E}}) = \vec{\boldsymbol{0}} \quad \text{and} \quad \operatorname{Div}(\vec{\boldsymbol{D}}) = 0. \tag{8}$$

The "pull-back" operation of the vector fields $\vec{\boldsymbol{e}}$ and $\vec{\boldsymbol{d}}$ reads

$$\vec{\boldsymbol{E}} = \boldsymbol{F}^T\vec{\boldsymbol{e}} \quad \text{and} \quad \vec{\boldsymbol{D}} = J\boldsymbol{F}^{-1}\vec{\boldsymbol{d}}, \tag{9}$$

respectively. In consequence of the conservative electric field, it can be expressed by a scalar field ϕ, called the potential of the electric field

$$\operatorname{curl}(\vec{\boldsymbol{e}}) = \vec{\boldsymbol{0}} \Rightarrow \vec{\boldsymbol{e}} = -\operatorname{grad}(\varphi) \quad \text{and} \quad \operatorname{Curl}(\vec{\boldsymbol{E}}) = \vec{\boldsymbol{0}} \Rightarrow \vec{\boldsymbol{E}} = -\operatorname{Grad}(\phi). \tag{10}$$

The scalar fields are composed together with $\phi = \varphi(\vec{\boldsymbol{\chi}}(\vec{\boldsymbol{X}}, t))$. Note that the negative sign is a convention.
Inside a dielectric material an applied electric field minimally separates the atomic nucleus and the electrons and it arise induced dipole moments. These moments align in the direction of the applied field. The dipole moments located on the microscopic scale are called on the macroscopic scale density of the electric dipole moments or polarization density, denoted by $\vec{\boldsymbol{p}}$. This quantity differs from zero only in electrically polarized matter and it's associated with the electric displacement field $\vec{\boldsymbol{d}}$ via the electric field $\vec{\boldsymbol{e}}$ through

$$\vec{\boldsymbol{d}} = \varepsilon_0\vec{\boldsymbol{e}} + \vec{\boldsymbol{p}} \quad \text{and} \quad \vec{\boldsymbol{D}} = \varepsilon_0 J\boldsymbol{C}^{-1}\vec{\boldsymbol{E}} + \vec{\boldsymbol{P}}, \tag{11}$$

where $\vec{\boldsymbol{P}} = J\boldsymbol{F}^{-1}\vec{\boldsymbol{p}}$ has been used. The permittivity of free space ε_0 has a defined value given approximately by $8.85419 \cdot 10^{-12}\ Fm^{-1}$ (measured in farads per meter). In a vacuum the electric displacement is related to the electric field by $\vec{\boldsymbol{d}}_0 = \varepsilon_0\vec{\boldsymbol{e}}_0$ or in the Lagrangian version through $\vec{\boldsymbol{D}}_0 = \varepsilon_0 J\boldsymbol{C}^{-1}\vec{\boldsymbol{E}}$. The polarization density, or briefly speaking the polarization $\vec{\boldsymbol{p}}$ could represent nonlinear or history dependent material behavior $\vec{\boldsymbol{p}}(\vec{\boldsymbol{e}}, ...)$ and as a result of Eq. (11), $\vec{\boldsymbol{d}}(\vec{\boldsymbol{e}}, ...)$, too. Here, this quantity will be only a function of the deformation $\boldsymbol{F}$ and electric field $\vec{\boldsymbol{e}}$,

$$\vec{\boldsymbol{p}} = \vec{\boldsymbol{p}}(\vec{\boldsymbol{e}}, \boldsymbol{F}) \quad \text{and} \quad \vec{\boldsymbol{P}} = \vec{\boldsymbol{P}}(\vec{\boldsymbol{E}}, \boldsymbol{F}). \tag{12}$$

Hence, a deformation process or/and an applied electric field could cause polarization and electric displacement.
Compared with this, in a linear, homogeneous, isotropic dielectric material the relation between the electric field and the polarisation results in $\vec{\boldsymbol{p}}_{lin.} = \varepsilon_0(\varepsilon_r - 1)\vec{\boldsymbol{e}}$. Here ε_r stands for the material specific relative permittivity (or dielectric constant). This parameter is only a static or scalar valued quantity for isotropic material, constant temperature and constant frequency. Plug in Eq. $(11)_1$ it follows:

$$\vec{\boldsymbol{d}}_{lin.} = \varepsilon\vec{\boldsymbol{e}} \quad \text{and with Eqs. } (11)_{1,2} \quad \vec{\boldsymbol{D}}_{lin.} = \varepsilon J\boldsymbol{C}^{-1}\vec{\boldsymbol{E}}. \tag{13}$$

Here $\varepsilon = \varepsilon_0\varepsilon_r$ represents the absolute permittivity.
In an electrically sensitive body an applied electric field is confined to polarization or electric displacement. An external electric field produces electrostatic forces $\vec{\boldsymbol{f}}_e$ in the

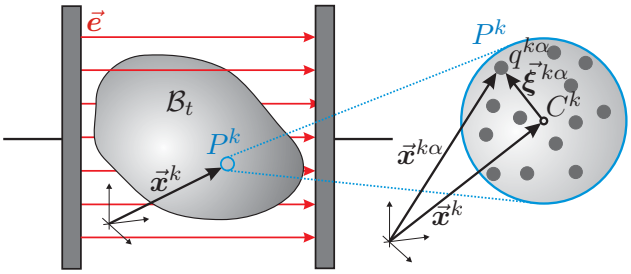

Figure 1: Macro- and microscopic scale of the considered body $\mathcal{B}_t$

continuum body $\mathcal{B}_t$. This volume force $\vec{f}_e$ can be derived from a microscopic scale. For this scale it is assumed that only pointwise sources exist. For the physical model a particle P^k of the current configuration $\mathcal{B}_t$ at position $\vec{x}^k$ is considered (see Figure 1). This particle contains elementary electric charge $q^{k\alpha}$ with mass $m^{k\alpha}$ at specific location $\vec{\xi}^{k\alpha}$ relative to the mass center C^k. At this level each randomly distributed charge within a particle interacts with other charges $\vec{e}_i$ and reacts on external electric fields $\vec{e}$. For further derivation internal interactions between the charges and influence of the gravitation field are neglected. Due to this the Lorentz force is given by $\vec{f}_L^{\,\alpha} = q^{k\alpha}\vec{e}(\vec{x}^{k\alpha})$. The external electric fields is expanded in a Taylor series, $\vec{e}(\vec{x}^{k\alpha}) = \vec{e}(\vec{x}^k) + \mathrm{grad}(\vec{e})\,\vec{\xi}^{k\alpha} + \ldots$, around x^k and a resultant electric force within the particle $\vec{f}_e^{\,k}$ can be derived by neglecting higher order terms

$$\vec{f}_e^{\,k} = \sum_{\alpha=1}^{n} q^{k\alpha}(\vec{e} + \mathrm{grad}(\vec{e}) \cdot \vec{\xi}^{k\alpha}) \tag{14}$$

with $\mathfrak{q}^k = \sum_{\alpha=1}^{n} q^{k\alpha}$ and $\vec{\mathfrak{p}}^k = \sum_{\alpha=1}^{n} q^{k\alpha}\vec{\xi}^{k\alpha}$ follows $\vec{f}_e^{\,k} = \mathfrak{q}^k\vec{e} + \mathrm{grad}^T(\vec{e})\,\vec{\mathfrak{p}}^k$. Here $\mathfrak{q}^k$ and $\vec{\mathfrak{p}}$ denotes the sum of the charge and polarisation within the particle P^k, respectively. Performing a simple space averaging leads to the macroscopic electric force per unit volume $\vec{f}_e = \rho_f\vec{e} + \mathrm{grad}^T(\vec{e})\,\vec{p}$. Where ρ_f is the free charge density and $\vec{p}$ the polarization density. This article assumes a material with no free charges and in this way it follows

$$\vec{f}_e = \mathrm{grad}^T(\vec{e})\,\vec{p}. \tag{15}$$

2.3 Equilibrium, stress and constitutive laws

For the sake of simplicity the further equations are given with respect to the current configuration. The mechanical body force density $\vec{f}_m$ as well as the acceleration are assumed to be zero. Then from the momentum balance principles the Cauchy equation of equilibrium can be deduced and reads

$$\mathrm{div}(\boldsymbol{\sigma}) + \vec{f}_e = \vec{\mathbf{0}}. \tag{16}$$

In the equation above, $\boldsymbol{\sigma}$ and $\vec{f}_e$ stand for the Cauchy stress tensor and the electric body force per unit current volume, respectively. The electric body force can be expressed as the divergence of a tensor, the electric, cauchy type, stress tensor $\boldsymbol{\tau}_e$

$$\vec{f}_e = \mathrm{div}(\boldsymbol{\tau}_e), \tag{17}$$

which is defined by

$$\boldsymbol{\tau}_e = \vec{e} \otimes (\varepsilon_0\vec{e} + \vec{p}) - \frac{1}{2}\varepsilon_0(\vec{e}\cdot\vec{e})\boldsymbol{I} = \underbrace{\varepsilon_0\left(\vec{e}\otimes\vec{e} - \frac{1}{2}(\vec{e}\cdot\vec{e})\boldsymbol{I}\right)}_{\boldsymbol{\tau}_M} + \vec{e}\otimes\vec{p}. \tag{18}$$

The first two terms in the latter equation denote the symmetric Maxwell stress tensor $\boldsymbol{\tau}_M$. The last term depends on the polarization of the considered material. A total Cauchy type stress tensor $\boldsymbol{\tau}$ is introduced,

$$\boldsymbol{\tau} = \boldsymbol{\sigma} + \boldsymbol{\tau}_e. \tag{19}$$

Therefore the Cauchy equation of equilibrium becomes

$$\operatorname{div}(\boldsymbol{\tau}) = \vec{\mathbf{0}}. \tag{20}$$

It can be shown that Eq. (20) fulfills Cauchy's second equation of motion (balance of angular momentum)

$$\boldsymbol{\mathcal{E}} : \boldsymbol{\tau} = \vec{\mathbf{0}}. \tag{21}$$

accordingly, the latter equation is no longer a constitutive equation and it follows that $\boldsymbol{\tau}$ is symmetric. The two dots characterize the double contraction. Pull-back operations relating to $\boldsymbol{\tau}$, lead to $\hat{\boldsymbol{P}} = J\boldsymbol{\tau}\boldsymbol{F}^{-T}$ and $\boldsymbol{T} = J\boldsymbol{F}^{-1}\boldsymbol{\tau}\boldsymbol{F}^{-T}$. Representing stress tensors of the first- and second Piola-Kirchhoff type, respectively. The mechanical part of the stress is defined by the first, $\boldsymbol{P} = J\boldsymbol{\sigma}\boldsymbol{F}^{-T}$, or second Piola-Kirchhoff stress tensor, $\boldsymbol{S} = J\boldsymbol{F}^{-1}\boldsymbol{\sigma}\boldsymbol{F}^{-T}$. For better legibility, further deliberations are given only with respect to the reference configuration.
There are different ways to introduce the constitutive equations. We will follow the methodology by Coleman and Noll [21], [22] to find the imposed conditions by the second law of thermodynamic. In this paper the electric field $\vec{\boldsymbol{E}}$ and the deformation $\boldsymbol{F}$ are the independent primary variables. For the internal dissipation inequality holds

$$\mathcal{D}_{int} = -\rho_0\dot{\psi} - \vec{\boldsymbol{P}} \cdot \dot{\vec{\boldsymbol{E}}} + [\boldsymbol{P} + \boldsymbol{F}^{-T}\vec{\boldsymbol{E}} \otimes \vec{\boldsymbol{P}}] : \dot{\boldsymbol{F}} + \sum_{k=1}^{m} \boldsymbol{\Xi}_k : \dot{\boldsymbol{\alpha}}_k \geq 0. \tag{22}$$

Within Eq. (22) denotes ψ the Helmholtz free energy and ρ_0 the reference mass density. The latter term on the left-hand side characterizes the internal dissipation $\mathcal{D}_{int}^{visco}$ in the material

$$\mathcal{D}_{int}^{visco} = \sum_{k=1}^{m} \boldsymbol{\Xi}_k : \dot{\boldsymbol{\alpha}}_k \geq 0 \quad \text{with} \quad \boldsymbol{\Xi}_k = -\rho_0 \frac{\partial \psi}{\partial \boldsymbol{\alpha}_k}. \tag{23}$$

Inserting $\boldsymbol{\alpha}_k = {}^k\boldsymbol{F}_v$ in Eqs. (22, 23) then $\boldsymbol{\Xi}_k$ can be interpreted as an nonequilibrium viscous stress. In addition, it should be noted that k represents the number of internal dissipation mechanism. In Eq. (22) $\psi(\boldsymbol{F}, \boldsymbol{E}, {}^k\boldsymbol{F}_v)$ the free energy function depends on the deformation, the referential electric field and the internal variable $\boldsymbol{F}_v$. Plug in the material time derivative of ψ in Eq. (22), it follows

$$-(\vec{\boldsymbol{P}} + \rho_0 \frac{\partial \psi}{\partial \vec{\boldsymbol{E}}}) \cdot \dot{\vec{\boldsymbol{E}}} + (\boldsymbol{P} + \boldsymbol{F}^{-T}\vec{\boldsymbol{E}} \otimes \vec{\boldsymbol{P}} - \rho_0 \frac{\partial \psi}{\partial \boldsymbol{F}}) : \dot{\boldsymbol{F}} - \sum_{k=1}^{m} \rho_0 \frac{\partial \psi}{\partial\, {}^k\boldsymbol{F}_v} : {}^k\dot{\boldsymbol{F}}_v \geq 0. \tag{24}$$

Here ψ is extended by the free energy in vacuum E_{space} to the augmented energy density function Ω

$$\Omega = \rho_0\psi + E_{space}. \tag{25}$$

The term of the energy in vacuum is determined by $E_{space} = -1/2\,\varepsilon_0 J(\vec{\boldsymbol{E}} \otimes \vec{\boldsymbol{E}}) : \boldsymbol{C}^{-1}$. The free energy W contains the elastic energy W_{elast} and the electric energy W_{elect}. In

the context of viscoelasticity the total energy Ω is additive enhanced by the viscoelastic energy W_{visco}. Note that for each internal dissipation mechanism k one energy function ${}^kW_{visco}$ has to be specified, k is a positive integer and runs from one to m.

$$\Omega = \overbrace{\underbrace{W_{elast} + W_{elect}}_{W} + E_{space}}^{W_{elel}} + {}^kW_{visco}. \tag{26}$$

The **el**astic-**el**ectric energy part W_{elel} is a function of the electric field and the deformation and contains the energy of free space E_{space}. The viscous energy part ${}^kW_{visco}$ is only a function of the viscous deformation.

$$W_{elel} = W_{elel}(\boldsymbol{C}, \vec{\boldsymbol{E}}) \quad \text{and} \quad {}^kW_{visco} = {}^kW_{visco}({}^k\tilde{\boldsymbol{C}}_e = {}^k\boldsymbol{F}_v^{-T}\tilde{\boldsymbol{C}}{}^k\boldsymbol{F}_v^{-1}). \tag{27}$$

To fulfill the inequality Eq. (22) for all rates of $\dot{\vec{\boldsymbol{E}}}$, $\dot{\boldsymbol{F}}$ and $\dot{\boldsymbol{F}}_v$ the following constitutive relations have to be satisfied or in other words, the use of the standard argument from Coleman and Gurtin leads to

$$\boldsymbol{T} = 2\frac{\partial\Omega}{\partial\boldsymbol{C}},\ \vec{\boldsymbol{P}} = -\frac{\partial W}{\partial\vec{\boldsymbol{E}}},\ \mathcal{D}_{int}^{visco} = -\sum_{k=1}^{m}\frac{\partial\,{}^kW_{visco}}{\partial\,{}^k\tilde{\boldsymbol{C}}_e} : \frac{\partial\,{}^k\tilde{\boldsymbol{C}}_e}{\partial\,{}^k\boldsymbol{F}_v} : {}^k\dot{\boldsymbol{F}}_v \geq 0$$
$$\text{and with Eq. } (11)_2\text{: } \vec{\boldsymbol{D}} = -\frac{\partial\Omega}{\partial\vec{\boldsymbol{E}}}. \tag{28}$$

This reduced dissipation inequality, $\mathcal{D}_{int}^{visco}$, is transformed with some mathematical operations into

$$-{}^k\boldsymbol{\tau}_{visco} : \frac{1}{2}\mathcal{L}_v({}^k\boldsymbol{b}_e)\cdot{}^k\boldsymbol{b}_e^{-1} \geq 0 \quad \text{with} \quad {}^k\boldsymbol{\tau}_{visco} = 2\frac{\partial\,{}^kW_{visco}}{\partial\,{}^k\boldsymbol{b}_e}\,{}^k\boldsymbol{b}_e. \tag{29}$$

Note that for further calculations and the numerical implementation m in Eq. $(28)_3$ equals one and for further derivations the superscript k is neglected. Here, τ_{visco} is the viscous Kirchhoff stress tensor. The notation $\mathcal{L}_v(\boldsymbol{b}_e)$ signify the Lie derivative of the elastic left Cauchy-Green tensor $\boldsymbol{b}_e = \boldsymbol{F}_e\boldsymbol{F}_e^T$ along the velocity field of the material motion. A solution strategy for Eq. (29) is given in subsection 3.3 or in detail in [13], [14]. Studying the free energy function Ω, the viscous free energy W_{visco} is only a function of the deformations. However, the total stress τ is deduced from the whole deformation $\boldsymbol{F}$.
With respect to isotropic material, W_{elel} is a scalar-valued isotropic tensor function of the two second-order tensor variables $\boldsymbol{C}$ and $\vec{\boldsymbol{E}}\otimes\vec{\boldsymbol{E}}$. The free energy function has to satisfy the condition to be unchanged if the material and the electric field undergo a rotation around a certain axis. Hence, W_{elel} is expressed as a function of the three invariants according to a hyperelastic material and three pseudo invariants of $\boldsymbol{C}$ and $\vec{\boldsymbol{E}}\otimes\vec{\boldsymbol{E}}$. This integrity base fulfills the above formulated condition and these are defined by

$$\tilde{I}_1 = \mathrm{tr}(\tilde{\boldsymbol{C}}) = J^{-2/3}I_1,\ \tilde{I}_2 = 1/2\left[\mathrm{tr}^2(\tilde{\boldsymbol{C}}) - \mathrm{tr}(\tilde{\boldsymbol{C}}^2)\right] = J^{-4/3}I_2,\ \tilde{I}_3 = 1,$$
$$I_4 = (\vec{\boldsymbol{E}}\otimes\vec{\boldsymbol{E}}) : \boldsymbol{I},\ I_5 = (\vec{\boldsymbol{E}}\otimes\vec{\boldsymbol{E}}) : \boldsymbol{C},\ I_6 = (\vec{\boldsymbol{E}}\otimes\vec{\boldsymbol{E}}) : \boldsymbol{C}^2. \tag{30}$$

Herein, tr(...) stands for the trace of a second-order tensor. Another integrity base can be found in [28],[29]. W_{elast} contains the isochoric and volumetric part of the elastic energy W_{iso} and W_{vol}, whereby $U_{vol} = dW_{vol}/dJ$ should be noted. An analytical study of the nonlinear equations gives a short overview over the interesting physical phenomenon. The electrical field produces polarization, $\partial W/\partial I_4 \neq 0$. The electrical field produces stress, $\partial W/\partial I_5 \neq 0$, the electrostrictive effect. The higher order tensor effect, $\partial W/\partial I_6 \neq 0$, is generally very small and normally not detectable in moderate fields [12].

2.4 Free energy function

In order to perform our analysis it is necessary to determine the energy function Ω. As already mentioned, the total free energy contains the elastic-electro energy part W, the viscoelastic energy W_{visco} and the term of the energy in vacuum E_{space}. It is assumed that the partial derivations of W with respect to I_4 and I_5 are positive constants ($W_{,4} = c_1,\ W_{,5} = c_2$). The derivation according to I_6 is neglected (see also subsection 2.3).

$$
\begin{aligned}
W_{elast}(\tilde{\lambda}_1, \tilde{\lambda}_2, \tilde{\lambda}_3, J) &= \frac{1}{4}\,\kappa\left(J^2 - 1 - \ln[J^2]\right) + \sum_{p=1}^{n} \frac{\mu_{pe}}{\alpha_{pe}}\left(\tilde{\lambda}_1^{\alpha_{pe}} + \tilde{\lambda}_2^{\alpha_{pe}} + \tilde{\lambda}_3^{\alpha_{pe}} - 3\right) \\
{}^{k}W_{visco}(\tilde{\lambda}_{1e}, \tilde{\lambda}_{2e}, \tilde{\lambda}_{3e}) &= \sum_{p=1}^{n} \frac{{}^{k}\mu_{pv}}{{}^{k}\alpha_{pv}}\left(\tilde{\lambda}_{1e}^{\,{}^{k}\alpha_{pv}} + \tilde{\lambda}_{2e}^{\,{}^{k}\alpha_{pv}} + \tilde{\lambda}_{3e}^{\,{}^{k}\alpha_{pv}} - 3\right), \quad k = 1, ..., m \\
W_{elect}(\boldsymbol{C}, \vec{\boldsymbol{E}}) &= c_1(\vec{\boldsymbol{E}} \otimes \vec{\boldsymbol{E}}) : \boldsymbol{I} + c_2(\vec{\boldsymbol{E}} \otimes \vec{\boldsymbol{E}}) : \boldsymbol{C} \\
E_{space}(\vec{\boldsymbol{E}}, J) &= -\frac{1}{2}\varepsilon_0 J(\vec{\boldsymbol{E}} \otimes \vec{\boldsymbol{E}}) : \boldsymbol{C}^{-1}
\end{aligned}
\tag{31}
$$

Here $\mu > 0$ and $\kappa > 0$ are interpreted as the shear modulus and the bulk modulus, respectively. Through a specific choice of the dimensionless constant $\alpha_{p(...)}$ (s. Eqs.$(31)_{1,2}$) and p it is possible to obtain Neo-Hookean-, Mooney–Rivlin-, and the Ogden material model.

3 Finite element implementation

The finite element method requires the formulation of the balance laws in form of variational formulations. They are denoted in the strong form with respect to the current and reference configuration. Two types of boundary conditions will be introduced. They are known as the Dirichlet and Neumann boundary conditions, which correspond to the displacement field $\bar{\vec{\boldsymbol{u}}}$ and electric scalar potential ϕ, the surface electric charge $\bar{\varsigma}$, and the total true traction vector $\bar{\vec{\boldsymbol{t}}}$ on the current surface $\partial\mathcal{B}_t$. By means of contrast, to this the displacement field and electric scalar potential, the surface electric charge, and the total nominal traction vector on the reference surface $\partial\mathcal{B}_0$ are named by $\bar{\vec{\boldsymbol{u}}}$ and ϕ, $\bar{\varsigma}$ and $\bar{\vec{\boldsymbol{T}}}$. The quantities $(\bar{...})$ are prescribed values which are necessary to solve the boundary value problem. The surface boundary $\partial\mathcal{B}$ is regarded as a discontinuous boundary.
With regards to the boundary surface, a distinction is made between the mechanical $\partial\mathcal{B}_m$ and electrical boundary $\partial\mathcal{B}_e$ with $\partial\mathcal{B} = \partial\mathcal{B}_e \cup \partial\mathcal{B}_m$. Therewith one has,

$$
\begin{gathered}
\partial\mathcal{B}_m = \partial_{\bar{\vec{\boldsymbol{u}}}}\mathcal{B} \cup \partial_{\bar{\vec{\boldsymbol{t}}}}\mathcal{B} \text{ and } \partial\mathcal{B}_e = \partial_{\phi}\mathcal{B} \cup \partial_{\varsigma}\mathcal{B} \\
\text{with disjoint parts } \partial_{\bar{\vec{\boldsymbol{t}}}}\mathcal{B} \cap \partial_{\bar{\vec{\boldsymbol{u}}}}\mathcal{B} = \emptyset \text{ and } \partial_{\varsigma}\mathcal{B} \cap \partial_{\phi}\mathcal{B} = \emptyset.
\end{gathered}
\tag{32}
$$

It should be mentioned that no surface charges $\bar{\varsigma}$ are considered and $\boldsymbol{\tau}\vec{\boldsymbol{n}} = \vec{\boldsymbol{t}}_a + \boldsymbol{\tau}_e\vec{\boldsymbol{n}}$. Where $\vec{\boldsymbol{t}}_a$ is the nonelectrical surface force per unit area.

3.1 Weak form

Multiplying the mechanical equilibrium Eq. (20) with the virtual displacement $\delta\vec{\boldsymbol{u}}$ and the Gauss law Eq. $(8)_2$ with the virtual electric potential $\delta\phi$ and integration over the volume of the considered body purveys the principle of virtual work. Here $\delta\vec{\boldsymbol{u}}$ is the kinematically admissible virtual displacement and $\delta\phi$ is the electrostatically admissible virtual electric potential. For reasons of clarity and comprehensibility the following weak

form is formulated in terms of the reference configuration

$$\mathcal{F}(\mathcal{F}(\vec{\boldsymbol{u}},\delta\vec{\boldsymbol{u}}),\mathcal{F}(\phi,\delta\phi)) := \int_{\mathcal{B}_0} \mathrm{Div}(\hat{\boldsymbol{P}})\cdot\delta\vec{\boldsymbol{u}}\,dV + \int_{\mathcal{B}_0} \mathrm{Div}(\vec{\boldsymbol{D}})\,\delta\phi\,dV = 0. \tag{33}$$

The use of integration by parts and following application of the divergence theorem, leads to the weak form of the equations above with build-in in von Neumann boundary conditions

$$\mathcal{F} = \underbrace{\int_{\mathcal{B}_0} \hat{\boldsymbol{P}} : \delta\boldsymbol{F}\,dV - \int_{\mathcal{B}_0} \vec{\boldsymbol{D}}\cdot\delta\vec{\boldsymbol{E}}\,dV}_{\mathcal{F}_{int}} - \underbrace{\left[\int_{\partial_{\vec{t}}\mathcal{B}_0} \vec{\bar{\boldsymbol{T}}}\cdot\delta\vec{\boldsymbol{u}}\,dA + \int_{\partial_{\varsigma}\mathcal{B}_0} \bar{\varsigma}\,\delta\phi\,dA\right]}_{\mathcal{F}_{ext}} = 0. \tag{34}$$

The terms $\mathcal{F}_{int}$ and $\mathcal{F}_{ext}$ denote the internal and external virtual work.

3.2 Discretization

For the use of the Finite Element Method (FEM) the continuous domain $\mathcal{B}_0$ is subdivided into n_e finite elements. The boundary $\partial\mathcal{B}_0$ is approximated by the surface of the outer elements. Within the numerical implementation we use an eight-node hexahedral "brick" element. In each element the displacement field $\vec{\boldsymbol{u}}$ and the electrical potential ϕ are approximated by the same shape functions N_I. In this way the body $\mathcal{B}_0^h$ is discretized by n_e elements. The nodal values of displacements and potential are represented by u_I and ϕ_I, so it holds

$$\mathcal{F}^e_{int} = \sum_{I=1}^{n_{en}} \left[\delta\vec{\boldsymbol{u}}_I \cdot \int_{\mathcal{B}_0} \hat{\boldsymbol{P}}\ \mathrm{Grad}(N_I)dV - \delta\phi_I \int_{\mathcal{B}_0} \vec{\boldsymbol{D}}\cdot\mathrm{Grad}(N_I)\,dV\right] \tag{35}$$

$$\mathcal{F}^e_{ext} = \sum_{I=1}^{n_{en}} \left[\delta\vec{\boldsymbol{u}}_I \cdot \int_{\partial_{\tau}\mathcal{B}_0} \vec{\bar{\boldsymbol{T}}} N_I\,dA + \delta\phi_I \int_{\partial_{\varsigma}\mathcal{B}_0} \bar{\varsigma}\,N_I\,dA\right]. \tag{36}$$

The isoparametric concept is used within this numerical implementation. Therefore, the geometry and the mentioned primary variables are interpolated by the same shape functions N_I.

3.3 Derivation and integration of the evolution law

We take up Eq. $(23)_1$ and one possibility to fulfill this inequality is, to transfer it in a positive definite quadratic form through an fourth-order tensor, $\mathcal{V}^{-1}$. From this it follows, that the evolution equation becomes

$$-\frac{1}{2}\mathcal{L}_v(\boldsymbol{b}_e)\cdot\boldsymbol{b}_e^{-1} = \mathcal{V}^{-1} : \boldsymbol{\tau}_{visco}. \tag{37}$$

The simplest way that $\mathcal{V}^{-1}$ could take is

$$\mathcal{V}^{-1} = \frac{1}{2\eta_{iso}}\left(\boldsymbol{\Pi} - \frac{1}{3}\boldsymbol{I}\otimes\boldsymbol{I}\right). \tag{38}$$

Through this specific choice it $\det[\boldsymbol{F}_v] = 1$ is a priori satisfied. Here, η_{iso} represents the isochoric material viscosity. Approximatively it holds $\tau = \frac{\mu_v}{\eta_{iso}}$ with $\mu_v = \frac{1}{2}\sum_{p=1}^{N}\mu_{pv}\alpha_{pv}$

for each nonequilibrium mechanism and τ represents the relaxation time. As a result of Eq. (46), Eq. (45) becomes

$$\mathcal{L}(\boldsymbol{b}_e) \cdot \boldsymbol{b}_e^{-1} = -\frac{1}{\eta_{iso}} \operatorname{dev}\left[\boldsymbol{\tau}_{visco}\right]. \tag{39}$$

Incidentally, $\operatorname{dev}[\ldots] = (\boldsymbol{\Pi} - 1/3\,(\boldsymbol{I} \otimes \boldsymbol{I})) : [\ldots]$ signify the deviatoric part of a second order tensor in the Eulerian description. Along with the forth order unit tensor $\boldsymbol{\Pi} = \delta_{ik}\delta_{jl}\,\vec{\boldsymbol{i}}_i \otimes \vec{\boldsymbol{i}}_j \otimes \vec{\boldsymbol{i}}_k \otimes \vec{\boldsymbol{i}}_l$. In the usual computational context the statement of the problem is regarded to be strain driven. Therefore the displacement is the primary variable. The quantities $\boldsymbol{F}_e$ and $\boldsymbol{F}_v$ have to be known, in order to deduce the stress. It is assumed that the deformation at the beginning of the time step $[t_n, t_{n+1}]$ is known through the start values $\{\boldsymbol{F}_{t_n}, \boldsymbol{b}_{e_{t_n}}\}$. The task is to determine the unknown kinematic tensors $\{\boldsymbol{F}_{t_{n+1}}, \boldsymbol{b}_{e_{t_{n+1}}}\}$. In this way the stress can be deduced through the viscoelastic potential W_{visco}. Note that in the computational context it is more efficient to work with $\{\boldsymbol{C}_{v_{t_n}}\}$ and $\{\boldsymbol{C}_{v_{t_{n+1}}}\}$, because the abovementioned unknowns could be replaced by Eq. $(5)_2$. To describe the viscoelastic deformation the time derivative of the spatial elastic deformation tensor, $\dot{\boldsymbol{b}}_e$, is used. If we assume that all conditions are known at the beginning of the calculation, then the problem can be divided into a purely elastic and viscous computation. Hence, this tensor is decomposed into an elastic predictor and inelastic corrector

$$\dot{\boldsymbol{b}}_e = \underbrace{\boldsymbol{l}\boldsymbol{b}_e + (\boldsymbol{l}\boldsymbol{b}_e)^T}_{\text{predictor}} + \underbrace{\mathcal{L}(\boldsymbol{b}_e)}_{\text{corrector}}. \tag{40}$$

To obtain the solution, the problem is divided in two steps. The integration of the first step is a priori satisfied, because all quantities are known. It follows $\boldsymbol{b}_{e_{trial}} = \boldsymbol{f}_{t_{n+1}} \boldsymbol{b}_{e_{t_n}} \boldsymbol{f}_{t_{n+1}}$. In this context $\boldsymbol{f}_{t_{n+1}} = \tilde{\boldsymbol{F}}\boldsymbol{F}_{t_n}^{-1}$ imply the relative deformation gradient. The total deformation gradient $\tilde{\boldsymbol{F}}$ within the iteration step is given due to the finite element approximation. With Eq. (45) it can be shown that the second step is a first order homogenous tensorial differential equation and can be solved for small time steps by the implicit (or backward) Euler integration method $\int_{t_n}^{t_{n+1}} (...)\, dt \approx \underbrace{(t_{n+1} - t_n)}_{\Delta t} \cdot (...)$

$$\boldsymbol{b}_{e_{t_{n+1}}} \approx \exp\left[-\frac{\Delta t}{\eta_{iso}} \operatorname{dev}\left[\boldsymbol{\tau}_{visco}\right]\right] \boldsymbol{b}_{e_{trial}}. \tag{41}$$

Note that this is a first order accurate approximation. The equation above can be formulated in principal directions λ_{Ae} of the left elastic deformation tensor and reads

$$\lambda^2_{Ae_{t_{n+1}}} \approx \exp\left[-\frac{\Delta t}{\eta_{iso}} \operatorname{dev}\left[\boldsymbol{\tau}_{visco}\right]\right] \lambda^2_{Ae_{trial}}. \tag{42}$$

So far there are three scalar equations which can be solved easily with the help of a local Newton iteration, which is performed on element level.
Afterwards $\boldsymbol{b}_{e_{t_{n+1}}} = \sum_{A=1}^{3} \lambda^2_{Ae_{t_{n+1}}} \vec{\boldsymbol{n}}_{A_{trial}} \otimes \vec{\boldsymbol{n}}_{A_{trial}}$ and viscous Kirchhoff stress $\boldsymbol{\tau}_{visco} = \sum_{A=1}^{3} (\partial W_{visco}/\partial \lambda_{Ae_{t_{n+1}}}) \lambda_{Ae_{t_{n+1}}} \vec{\boldsymbol{n}}_{A_{trial}} \otimes \vec{\boldsymbol{n}}_{A_{trial}}$ can be calculated. Here $\vec{\boldsymbol{n}}_{A_{trial}}$ and $\lambda_{Ae_{trial}}$ arise from a eigenvalue analysis of $\boldsymbol{b}_{e_{trial}}$. It holds $\vec{\boldsymbol{n}}_{A_{trial}} = \vec{\boldsymbol{n}}_{A_{t_{n+1}}}$.

3.4 Linearization

For an efficient numerical strategy to solve the nonlinear system of Eq. (35) and Eq. (36) Newton's method is used. Hence, the variational formulation $\mathcal{F}$ is expanded in a Taylor series and truncated after the linear part $\Delta\mathcal{F}$

$$\mathcal{F} + \Delta\mathcal{F} = 0. \tag{43}$$

This requires the computation of a consistent tangent by a linearization of the set of equations. The total traction $\vec{\bar{t}}$ and the surface charge $\bar{\varsigma}$ are treated as being independent of the the deformation of the body. Therefore, only the internal work $\mathcal{F}_{int}$ needs to be linearized by the following mathematical operation:

$$\Delta\mathcal{F} = \Delta_{\vec{u}}\mathcal{F}(\vec{u}) + \Delta_{\phi}\mathcal{F}(\phi) = \frac{d}{ds}\mathcal{F}(\vec{u} + s\,\Delta\vec{u})|_{s=0} + \frac{d}{ds}\mathcal{F}(\phi + s\,\Delta\phi)|_{s=0}. \tag{44}$$

Applying that to the variational formulation of the internal work, Equation (35) can be rewritten as

$$\begin{aligned}\Delta\mathcal{F}^{e}_{int} = &\int_{\mathcal{B}_0} \boldsymbol{T} : \Delta_{\vec{u}}\delta\boldsymbol{C}\, dV + \int_{\mathcal{B}_0} \delta C : \mathcal{M} : \Delta_{\vec{u}} C\, dV + \int_{\mathcal{B}_0} \delta\boldsymbol{C} : \mathcal{K} \cdot \Delta_{\phi}\vec{\boldsymbol{E}}\, dV \\ &+ \int_{\mathcal{B}_0} \delta\vec{\boldsymbol{E}} \cdot \mathcal{K}^{T} : \Delta_{\vec{u}}\boldsymbol{C}\, dV + \int_{\mathcal{B}_0} \delta\vec{\boldsymbol{E}} \cdot \mathcal{A}\, \Delta_{\phi}\vec{\boldsymbol{E}}\, dV.\end{aligned} \tag{45}$$

The material version of the accompanying fourth, third and second order tensors $\mathcal{M} = 4\frac{\partial^2\Omega}{\partial\boldsymbol{C}\partial\boldsymbol{C}}$, $\mathcal{K} = -2\frac{\partial^2\Omega}{\partial\boldsymbol{C}\,\partial\vec{\boldsymbol{E}}}$, $\mathcal{K}^T = -2\frac{\partial^2\Omega}{\partial\vec{\boldsymbol{E}}\,\partial\boldsymbol{C}}$ and $\mathcal{A} = \frac{\partial^2\Omega}{\partial\vec{\boldsymbol{E}}\,\partial\vec{\boldsymbol{E}}}$ can be found in [23, 19] for the elastic and electric energy function. Further calculations and the built in shape-functions lead to the algorithmic tangent. Here $N_{(...),k}\,, k = 1, ..., 3$ represents the derivation of N with respect to the i-th direction. The linearization of the viscous part of the algorithm tangent is not elucidated, which is relevant for the second term in Eq. (45). This issue can be found in [13].

4 Numerical examples

The objective of this section is to show examples for the introduced nonlinear visco-electroelastic model. In the context of visco-electroelasticity the material behavior appears to deform permanently under the influence of an electrical loading. By analogy to the permanent deformation under an mechanical loading, we will also speak from retardation.

4.1 Thick-walled spherical shell under an electric field

In the first example we consider a thick-walled spherical shell under the influence of an electric field in order to validate the pure electroelastic model. Note that no viscous effects are considered in this example.
In the finite element solution, the spherical shell is modeled by elements with trilinear shape functions and a Neo-Hookean material model is used (see Figure 2). Due to the lack of experimental and material data the material and electromechanical parameters are occasionally defined and are shown on the right-hand side in Figure 2. Symmetry is considered in the numerical solution by modeling only one eighth of the sphere. The shell is discretized with 144 elements in tangential direction and, for a convergency study, with 2-10 elements in radial direction. Symmetry boundary conditions are utilized, in order to achieve a the shell fixed in both tangential directions. Two cases will be studied. In the first case (Case I) the shell is fixed at the boundaries in radial direction. The second case (Case II) investigates a fixed inner surface and a moveable outer surface in radial direction. In both cases, the shell is loaded by a radial electrical field of $10\,V/mm$. The inner surface is grounded, on the outer surface a voltage of $10\,V$ is applied. Note that this problem is a one-dimensional problem and other segmentations are possible. In reference to the spherically symmetrical loading, the electric potential is only a function of radius R. Furthermore, the offset diagonals of the stress tensor are zero and the principal stresses

are equal, because of the mentioned loading and the use of spherical coordinates. The spherical coordinates in the undeformed configuration are (R, Θ, Φ), and (r, θ, φ) during the deformation. The reference geometry is defined by

$$R_i \leq R \leq R_o,\ 0 \leq \Theta \leq \pi,\ 0 \leq \Phi \leq 2\pi$$

whereas R_i and R_o are the inner and outer radii of the shell, respectively. The current

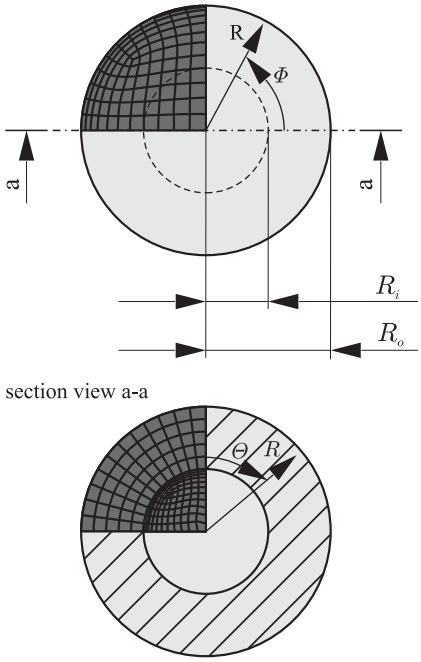

geometry	
inner radius	$R_i = 10\,mm$
outer radius	$R_o = 20\,mm$
electrical parameters	
inner potential	$\phi(r(R_i)) = 0\,V$
outer potential	$\phi(r(R_o)) = 10\,V$
material parameters	
mechanical	
shear modulus	$\mu = 5\,Nmm^{-2}$
bulk modulus	$\kappa = 16\,Nmm^{-2}$
electrical	
parameter	$c_1 = 10\,Fmm^{-1}$
parameter	$c_2 = 6\,Fmm^{-1}$

Figure 2: Geometry and finite element mesh of thick-walled spherical shell

geometry is described by

$$r_i \leq r \leq r_o,\ 0 \leq \theta \leq \pi,\ 0 \leq \varphi \leq 2\pi.$$

With the fundamental equations $\mathrm{Div}(\vec{\boldsymbol{D}}) = 0$ and $\mathrm{Div}(\hat{\boldsymbol{P}}) = 0$ the system of equations follows

$$\begin{aligned} \frac{\partial \hat{P}_{RR}}{\partial R} + \frac{2}{R}(\hat{P}_{RR} - \hat{P}_{\Theta\Theta}) &= 0 \\ \frac{\partial D_R}{\partial R} + \frac{2}{R} D_R &= 0. \end{aligned} \tag{46}$$

See [7] for an arbitrary vector and tensor in spherical coordinates. D_R is the only non-zero component of the electric displacement vector. The component of the stress tensor $\hat{P}_{RR}$ is the principal stress in radial direction. The components $\hat{P}_{\Theta\Theta}$ and $\hat{P}_{\Phi\Phi}$ are the principal stress components in tangential direction, with $\hat{P}_{\Theta\Theta} = \hat{P}_{\Phi\Phi}$. The aforementioned system of differential equations and the boundary conditions $r(R_i)$, $r(R_o)$, $\phi(r(R_i))$ and $\phi(r(R_o))$ complete the boundary value problem. Take into a account, that the free energy in a vacuum and higher order effects are neglected $E_{space} = 0$ and $W_{,6} = 0$, respectively. From this it follows that $\Omega = W$ and $\vec{\boldsymbol{P}} = \vec{\boldsymbol{D}}$. The first Piola-Kirchhoff type stress tensor $\hat{\boldsymbol{P}} = \boldsymbol{F}\boldsymbol{T}$ and the electric displacement $\vec{\boldsymbol{D}}$ can be derived:

$$\begin{aligned} \hat{\boldsymbol{P}} &= 2\boldsymbol{F}\left[J^{-2/3}\mathbb{P} : \tilde{W}_{,1}\boldsymbol{I} + \tilde{W}_{,2}\left(\tilde{I}_1\boldsymbol{I} - \tilde{\boldsymbol{C}}\right) + 1/2JU_{vol,\,J}\boldsymbol{C}^{-1} + W_{,5}\vec{\boldsymbol{E}} \otimes \vec{\boldsymbol{E}}\right] \\ \vec{\boldsymbol{D}} &= -2(W_{,4}\vec{\boldsymbol{E}} + W_{,5}\boldsymbol{C}\,\vec{\boldsymbol{E}}). \end{aligned} \tag{47}$$

Through the choice of a Neo-Hookean material model for the derivations of the free energy function W holds

$$\tilde{W}_{,1} = \mu/2,\ \tilde{W}_{,2} = 0,\ U_{vol} = \kappa/4\,(J^2 - 1 - \ln[J^2]),\ W_{,4} = c_1,\ W_{,5} = c_2. \tag{48}$$

The deformation gradient and related quantities can be expressed in spherical coordinates as follows

$$\boldsymbol{F} = \begin{pmatrix} r' & 0 & \\ 0 & r/R & 0 \\ 0 & 0 & r/R \end{pmatrix},\ \boldsymbol{C} = \boldsymbol{b} = \begin{pmatrix} r'^2 & 0 & \\ 0 & (r/R)^2 & 0 \\ 0 & 0 & (r/R)^2 \end{pmatrix},\ J = \left(\frac{r}{R}\right)^2 r', \tag{49}$$

where $r' = \frac{\partial r(R)}{\partial R}$. Now it is possible to obtain all non-zero components of the stress tensor and the electric displacement through Eqs. $(46)_{1,2}$, (47) and (48).

$$\begin{aligned}
\hat{P}_{RR} &= \frac{2}{3}\mu\left[r'^{1/3}\left(\frac{r(R)}{R}\right)^{-4/3} - r'^{-5/3}\left(\frac{r(R)}{R}\right)^{2/3}\right] + \frac{\kappa}{2}\left[r'\left(\frac{r(R)}{R}\right)^{4} - r'^{-1}\right] + 2c_2 r' E_r^2 \\
\hat{P}_{\Theta\Theta} &= \frac{1}{3}\mu\left[r'^{-2/3}\left(\frac{r(R)}{R}\right)^{-1/3} - r'^{4/3}\left(\frac{r(R)}{R}\right)^{-7/3}\right] + \frac{\kappa}{2}\left[r'^2\left(\frac{r(R)}{R}\right)^{3} - \left(\frac{r(R)}{R}\right)^{-1}\right] \\
D_R &= -2c_1 E_r - 2c_2 r'^2 E_r
\end{aligned} \tag{50}$$

The nodal displacements in radial direction are depicted in Figure 3 for the different

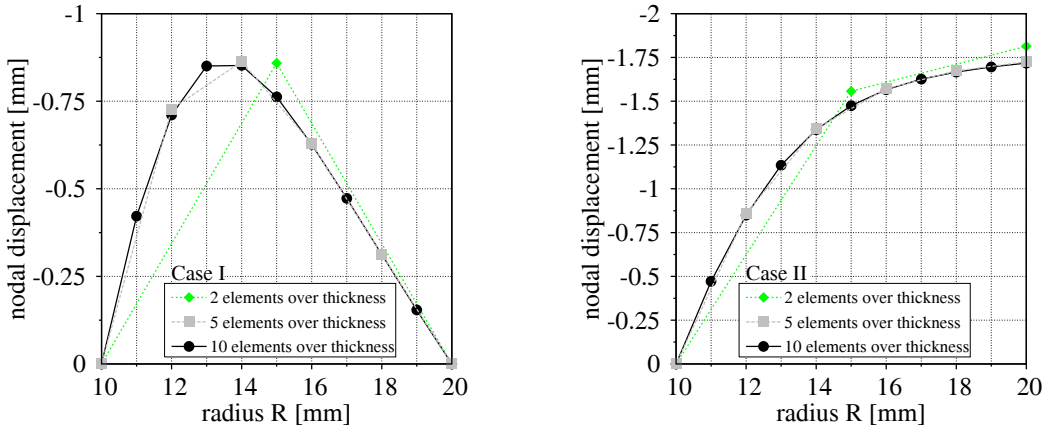

Figure 3: Displacement vs. radius for Case I (left) and Case II (right)

boundary conditions. As a result, further calculations are performed using by five elements over the thickness.

In Figure 4, the finite element results are compared with the above-mentioned analytical approach. The solution for Eqs. $(46)_{1,2}$ with the two different boundary conditions (Case I and Case II) was found by Maple™[2](Waterloo, ON, Canada). In the left diagram in Figure 4, the radius in the current configuration $r(R)$ vs. the electric potential ϕ is plotted. In the right, the radius in the current configuration $r(R)$ is depicted against the radius in the reference configuration. The dashed curve implies in each case the initial situation. The solid curves describe the results found by the analytical method and the dotted curves elucidate the finite element solutions of the proposed model. A horizontal line from the dashdotted curve to one of the solid or dotted curves can be interpreted as the difference between reference and current configuration. In comparison to the analytical

[2]Maple is a trademark of Waterloo Maple Inc.

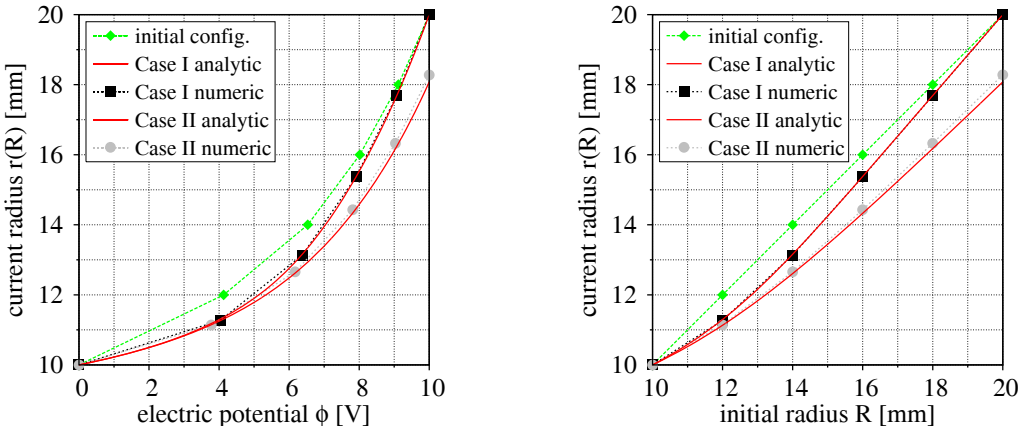

Figure 4: Current radius versus electric potential (left) and the current radius versus initial radius (right) of the spherical shell

approach the results matches for both boundary conditions. The last picture (see Figure 5) in this subsection shows the convergence behavior of the ten load steps for both cases.

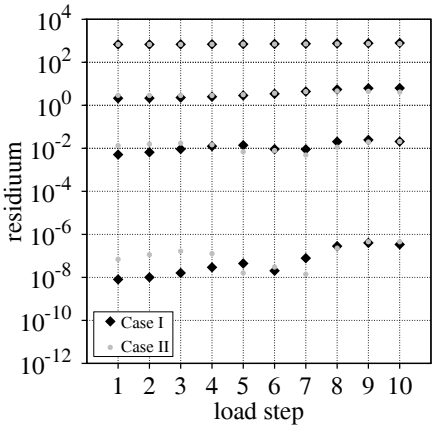

Figure 5: Residuum versus load step for five elements over thickness for Case I and Case II of the spherical shell

4.2 Plate under electrical loading

In this example a plate with a centered hole is analyzed under the influence of an electric potential. A similar example has been presented in [23] in the context of nonlinear electroelasticity. Only one eighth of the plate is discretized and symmetry boundary conditions are utilized (see Figure 6). A potential of $\phi = 220\,V$ is applied at the top end of the plate. The bottom end is grounded. Therefore an electric field of $5.5\,V/mm$ is brought up and for reasons of symmetry the plate is loaded with $\phi = 110\,V$. Along with the material parameters, the loading conditions are listed on the right-hand side of Figure 6. In this example the Neo-Hookean material model ($p = 1$, cf Eq. $(31)_1$) and one viscoelastic process with $m = 1$, cf Eq. $(31)_2$ is used. The electrical loading is applied from $0\,V$ to $110\,V$ in ten time steps to $\Delta t = 0.01\,s$ (s. right axis of ordinates in Figure 8). After applying this linear increasing electrical load, the electric potential is held fixed until $t = 10\,s$ at time steps of $\Delta t = 0.1\,s$. The convergence behavior is studied with four different meshes with 8, 64, 512, and 1600 elements. This corresponds to 81, 435, 2727, and 7689 degrees of freedom in the FE-analysis, respectively. The results are presented on the left-hand side of Figure 7. As a

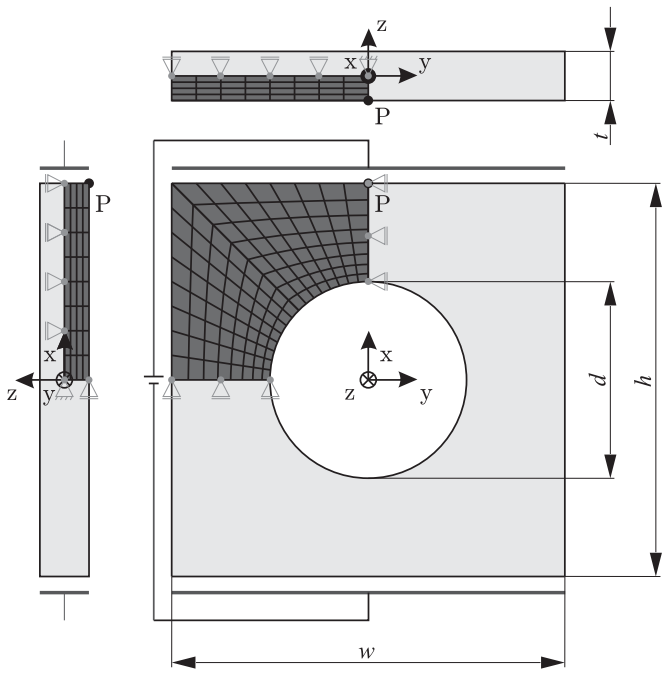

geometry	
height	$h = 40\,mm$
width	$w = 40\,mm$
diameter	$d = 10\,mm$
thickness	$t = 5\,mm$
loading conditions	
elec. pot. at $x = 20\,mm$	$\phi = 220\,V$
elec. pot. at $x = -20\,mm$	$\phi = 0\,V$
material parameters	
mechanical	
in Eqs. $34_{1,2}$	$n = 1$
in Eq. 34_2	$m = 1$
elastic shear modulus	$\mu_{1e} = 5\,N/mm^{-2}$
bulk modulus	$\kappa = 6.67\,N/mm^{-2}$
viscous shear modulus	${}^1\mu_{1v} = 5\,N/mm^{-2}$
viscosity	${}^1\eta_{iso} = 1, 10$ or $100\,Ns\,mm^{-2}$
additional parameter	$\alpha_{1e} = \alpha_{1v} = 2$
electrical	
parameter	$c_1 = 0.01\,Fmm^{-1}$
parameter	$c_2 = 0.06\,Fmm^{-1}$

Figure 6: Geometry, finite element mesh (left); loading conditions and material parameters (right) of the plate

consequence all further calculations are done by a plate modeled with 512 elements. As an example the order of convergence for the first 15 load steps is depicted on the right-hand side of Figure 7. The results of the finite element analysis are presented in Figure 8 for different values of the viscosity $\eta_{iso} \in (1, 10, 100)\,Ns\,mm^{-2}$. Here, the displacement in x-direction in millimeter $[mm]$, measured at point P at (x, y, z) $= (20\,mm, 0\,mm, -2.5\,mm)$ (see Figure 6), vs. the time in seconds $[s]$ is depicted. Figure 8 clearly illustrates the viscoelastic effects of the formulation. This implies that electric fields leads to creep effects in the material. The first picture in Figure 9 shows the distribution of the electric potential and the vectors illustrate the electric displacement. The remaining pictures in Figure 9 illustrate the distribution of the displacements. The stresses caused by the electrical loading are exemplified in Figur 10. Results in Figure 9 and 10 are calculated for the case ${}^1\eta_{iso} = 1\,Ns\,mm^{-2}$ and after the end of loading ($t = 10\,s$) based on a model with 512 elements.

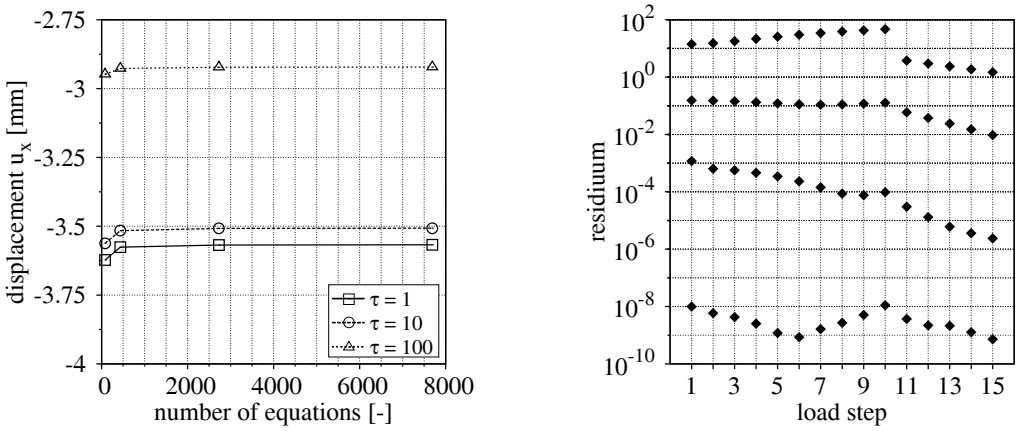

Figure 7: Convergence of displacement measured at point P of the plate with increasing number of elements for ${}^1\eta_{iso} = 1\,Ns\,mm^{-2}$, ${}^1\eta_{iso} = 10\,Ns\,mm^{-2}$ and ${}^1\eta_{iso} = 100\,Ns\,mm^{-2}$ (left); Residuum order exemplary for the first 15 load increments and ${}^1\eta_{iso} = 1\,Ns\,mm^{-2}$ (right).

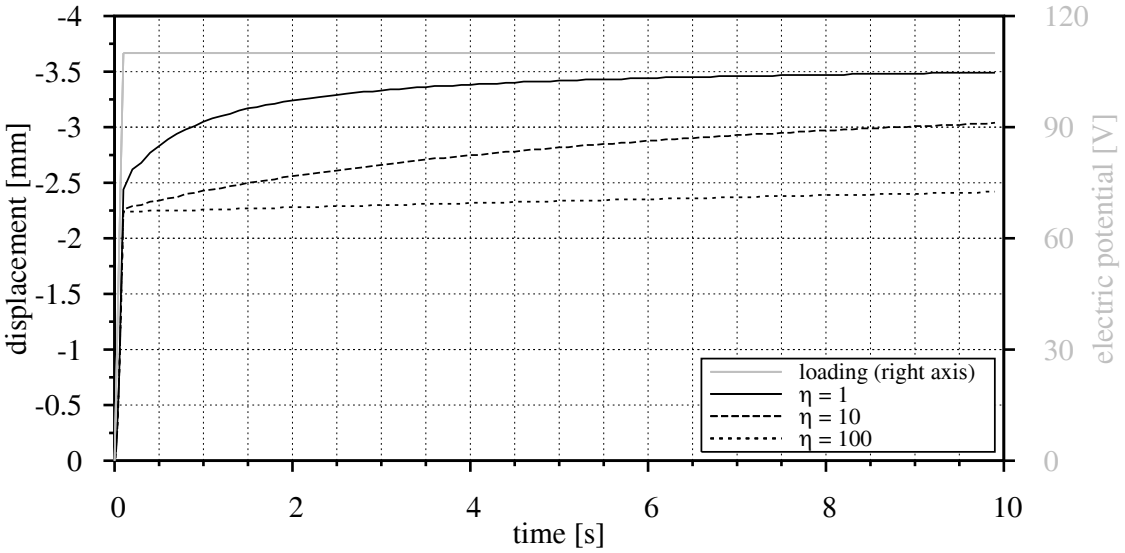

Figure 8: Retardation curves for the different retardation times ${}^1\eta_{iso} = 1\,Ns\,mm^{-2}$, ${}^1\eta_{iso} = 10\,Ns\,mm^{-2}$ and ${}^1\eta_{iso} = 100\,Ns\,mm^{-2}$.

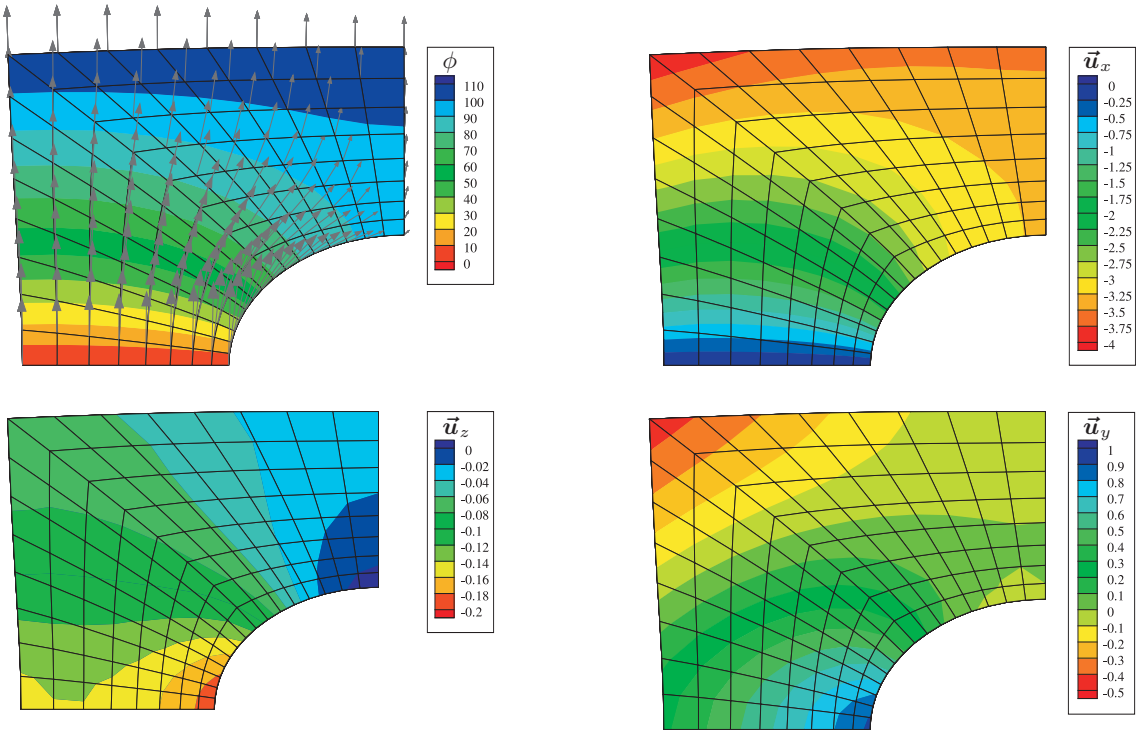

Figure 9: Electric potential ϕ in $[V]$, the electric displacement $\vec{\boldsymbol{d}}$ (vectors) (top left) and the displacements in x, y, z-direction in $[mm]$ in the deformed configuration for $\eta_{iso} = 1\,Ns\,mm^{-2}$

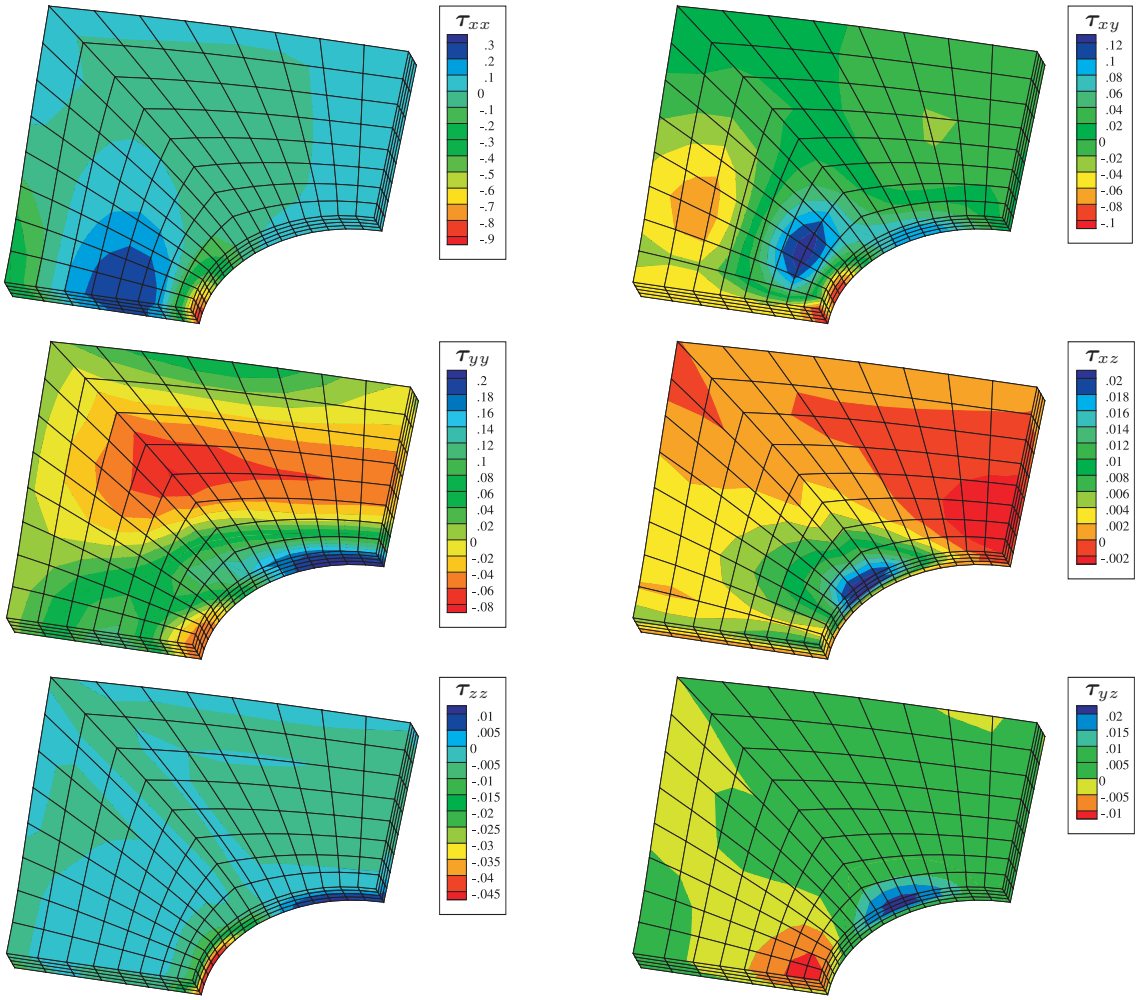

Figure 10: In each case $\eta_{iso} = 1\,Ns\,mm^{-2}$ in the deformed configuration: counterclockwise from top left: $\boldsymbol{\tau}_{xx}$, $\boldsymbol{\tau}_{yy}$, $\boldsymbol{\tau}_{zz}$, $\boldsymbol{\tau}_{yz}$, $\boldsymbol{\tau}_{xz}$, and $\boldsymbol{\tau}_{xy}$ in $[N/mm^2]$.

4.3 Tubular actuator

In this example a idealized tubular actuator made of electroactive polymers is investigated. The specimen is based on an actuator from Danfoss Polypower A/S, Denmark, which is already commercially available. Progress in research and development in the field of active polymers has enabled the fabrication of this new active material, which demonstrates the future potential and versatility of this technology. Tubular actuators are also referred to as rolled, coiled or wrapped actuators. In this example the loading conditions are variable, whereas in the previous example the retardation time τ or the boundary conditions have been changed. The left-hand side of Figure 11 shows the setup for this type of actuator.

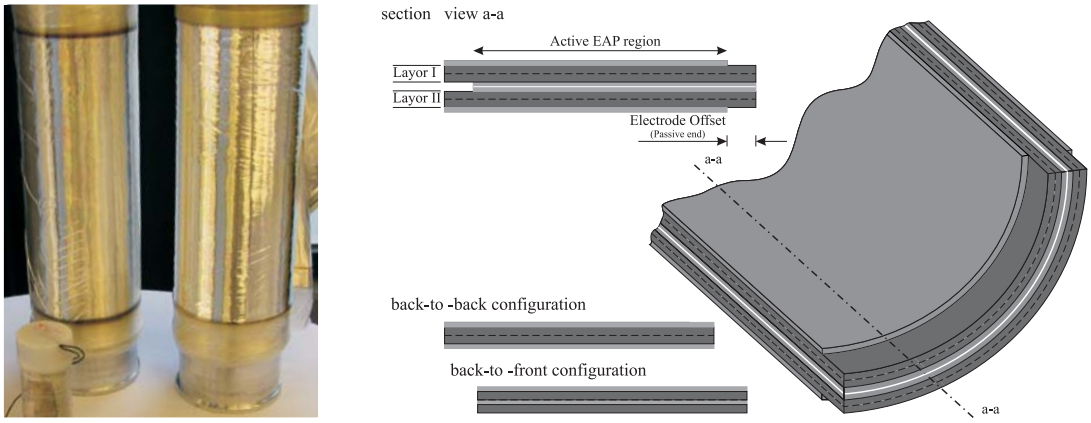

Figure 11: Unclad InLastor®from Danfoss Polypower A/S, Denmark (left) and schematic structure of a four-layer composite EAP laminate (right).

This involves winding dielectric polymer film (silicon elastomer) with a thickness of $80\,\mu m$ around a mandrel. One of the two surfaces of this elastomer film is corrugated and the electrode is applied onto it. The compliant electrode consists of the noble metal silver (Ag) with a thickness of $100\,nm$. On the right-hand side of Figure 11 the active film has dark shading and the electrode has lighter shading. In this picture, a back-to-back configuration of the layers, is depicted. Two identical back-to-back laminates (Layer I and II) are laminated together to form a four-layer composite assembly. Figures 12 and 13 show the approximated geometry and structure of the actuator, which consists of coiled active and passive layers. The active layer has dark shading. The separating layer (passive) inbetween is highlighted in grey. In the finite element analysis 240 elements are used for the cross section. In axial direction 4, 8 or 16 elements are used for a convergence study. The results are shown in Figure 14 and as a consequence 16 elements in axial direction are used for further calculations. The active elements are based on the presented model. Nonconducting geometrical nonlinear hexahedron elements with linear shape-functions are used for the passive layer. The specimen is loaded with a sinusoidal electrical potential with different frequencies. The amplitude of the loading is $2500\,V$ and the variable frequencies are 0.1 Hz, 1 Hz and 10 Hz. This Voltage is applied on the inner surface of the active layer. The outer surface of the active layer is grounded. The material parameters are chosen from preceding example. A Neo-Hookean material model and one viscoelastic process is used, $(p = 1)$ and $(m = 1)$ in Eqs. $(35)_{1,2}$), respectively. The material parameters μ and κ originate from a product data sheet of the aforementioned company. For the following diagrams, the displacement is measured at the top end of the actuator at point P (x= $1\,mm$, y= $0\,mm$, z= $8\,mm$) (see Figure 12 or 13). All remaining parameters which were used for the simulation are defined in Figure 12. The specimen is clamped at the bottom end (z= $0\,mm$). At the top end (z=$8\,mm$), only axial displacements

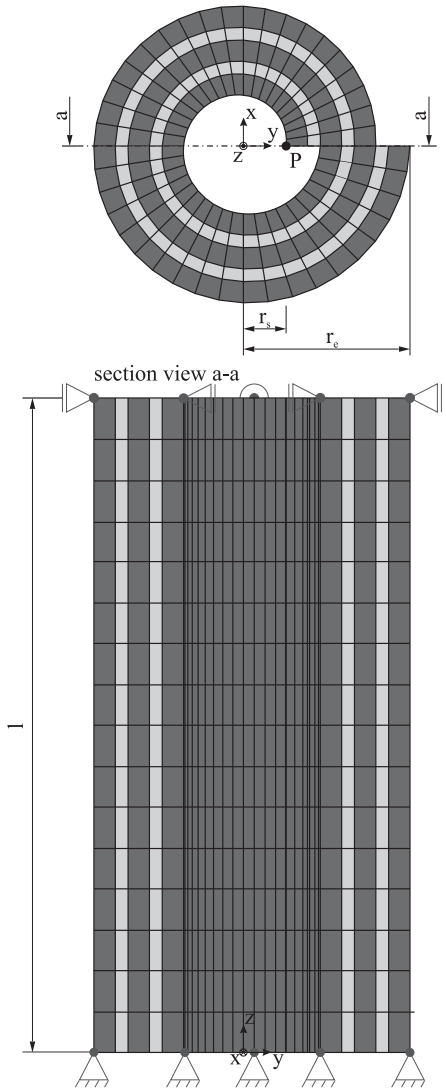

geometry	
length	$l = 8\,mm$
starting radius	$r_s = 1\,mm$
ending radius	$r_e = 4\,mm$
loading conditions	
elec. pot. inner surface	$\phi = 2500\,V$
elec. pot. outer surface	$\phi = 0\,V$
passiv layer	
layer thickness	$t = 0.3\,mm$
materials parameters	
shear modulus	$\mu = 0.37\,N/mm^{-2}$
bulk modulus	$\kappa = 18.33\,N/mm^{-2}$
active layer	
layer thickness	$t = 0.5\,mm$
materials parameters	
in Eqs. $(31)_{1,2}$	$n = 1$
in Eq. $(31)_2$	$k = 1$
elastic shear modulus	$\mu_{1e} = 0.37\,N/mm^{-2}$
bulk modulus	$\kappa = 18.33\,N/mm^{-2}$
viscous shear modulus	${}^1\mu_{1v} = 0.37\,Nmm^{-2}$
viscosity	${}^1\eta_{iso} = 10\,Ns\,mm^{-2}$
parameter α	$\alpha_{1e} = {}^1\alpha_{1v} = 2$
material-electrical parameters	
parameter	$c_1 = 2.7 \cdot 10^{-8}\,Fmm^{-1}$
parameter	$c_2 = 2.7 \cdot 10^{-8}\,Fmm^{-1}$

Figure 12: Geometry, finite element mesh, loading conditions and material parameters of the actuator

are possible. At this end, nodes are linked together, to have identical displacements. On the right-hand side of Figure 14 the displacement u_z is plotted for $90\,s < t < 100\,s$. It shows the obvious time-dependent reaction of the material. The displacement u_z vs. time is depicted in Figure 15. It points out the influence of the viscosity through the time dependent retardation of the displacement. The dissipative effects can be seen in the hysteresis curves from Figure 15. These diagrams show the electric potential ϕ over the displacement u_z. It is evident, that the dissipative effect is greater for low frequencies than for high frequencies. A further point, which can be seen in Figure 15, is the quadratic effect in the formulation. Due to the sinusoidal electric loading, the direction of the electric field switches, but due to electrostriction the displacement doesn't change the direction.

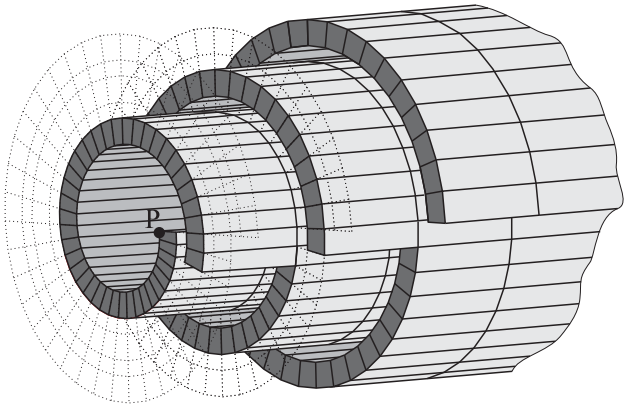

Figure 13: The nonlinear visco-electroelastic elements have dark shading and the electric loaded surface (active layer) has light shading. The nonconducting elements (passive layer) between the active layers are not drawn

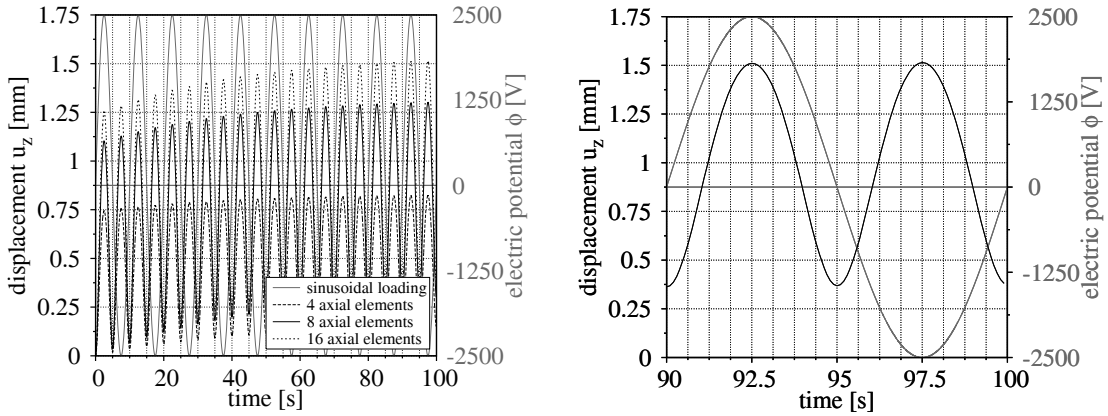

Figure 14: Right: displacement u_z for variable number of axial elements by frequency of $f_1 = 0.1\,Hz$. Left: displacement u_z for the first $10\,s$ loaded by $2500\,V$. For both graphs $f_1 = 0.1\,Hz$ and 16 axial elements are used

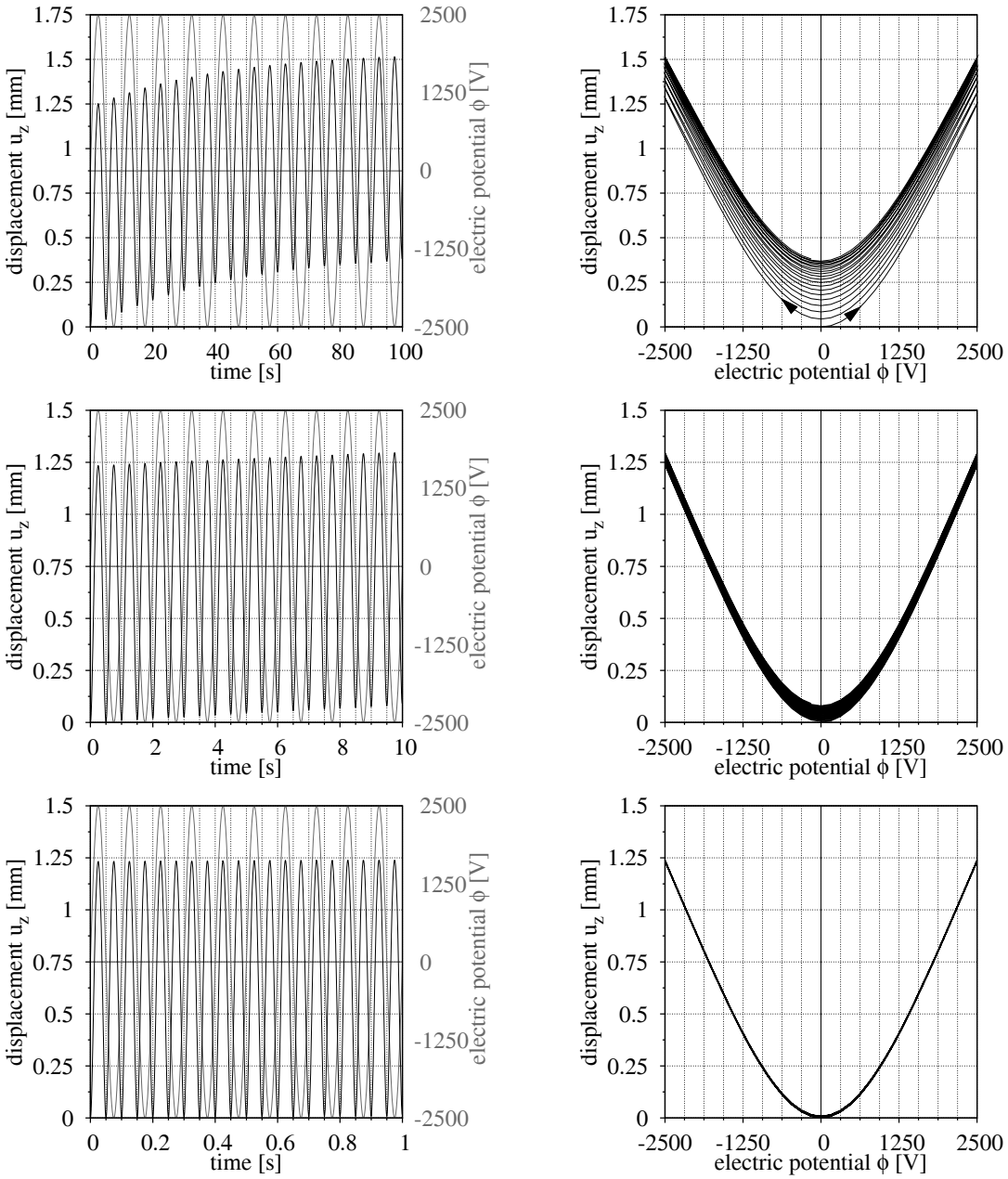

Figure 15: Displacement u_z vs. time for different frequencies $f_1 = 0.1\,Hz$, $f_2 = 1\,Hz$ and $f_3 = 10\,Hz$

4.4 Circular dielectric electro active polymer actuator

Finally, a circular actuator is considered and its response to pre-strain and electrical loading is analyzed. It consists of the circular elastomer and a solid frame. The electrodes are attached on the bottom side and top side of the circular slab-like dielectric elastomer, see Figure 16. The Dielectric electroactive polymer (DEAP) has a outer diameter of $d_o = 22\,mm$ and an inner of $d_i = 12.5\,mm$. The elastomer and the electrodes are approximately $h_d = 40\,\mu m$ and $h_e = 10\,\mu m$ thick, respectively. The specimen reacts to an electric field with an out of plane motion of the center plate, compare both pictures in Figure 16. For a more detailed description, we refer to the experimental papers [33, 34]. For the finite

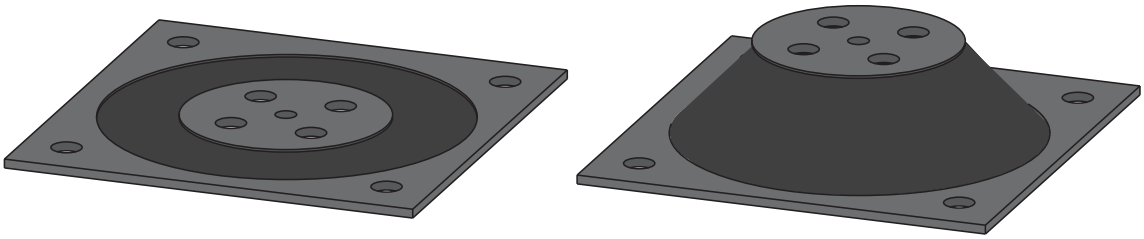

Figure 16: Circular actuator in the initial and deformed configuration.

element simulation only one quarter of the elastomer is modeled. Note that, due to the lack of material parameters for the electrode material, we do not consider the electrodes in the simulation. The outer edge of the elastomer is rigidly adhered to the solid frame and the inner edge is rigidly adhered to the circular slab. The displacement degrees of freedom on the edges in radial direction are constrained. However, the inner edge is allowed to move in z-direction. Ten Elements in radial direction and twenty elements

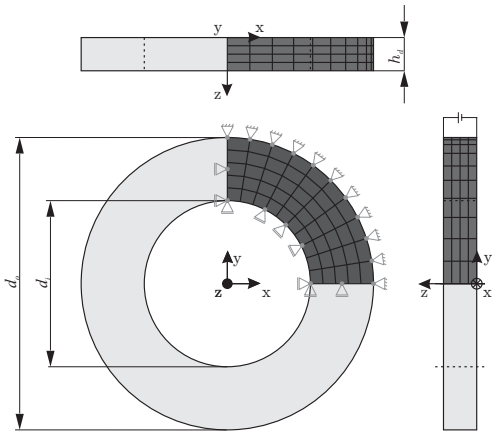

material parameters

dielectrica

in Eqs. $(31)_{1,2}$	$n = 1$
in Eq. $(31)_2$	$k = 1$
shear modulus and	$\mu_{1e} = 2.03\text{E}{-2}\,Nmm^{-2}, \alpha_{1e} = 2.71$
parameter α	$\mu_{2e} = 1.47\text{E}{-5}\,Nmm^{-2}, \alpha_{2e} = 15.27$
	$\mu_{3e} = -0.23\,Nmm^{-2}$ $, \alpha_{3e} = -8.79$
	$\mu_{1v} = 0.75 \cdot \mu_{1e}$ $, \alpha_{1v} = \alpha_{1e}$
	$\mu_{2v} = 0.75 \cdot \mu_{2e}$ $, \alpha_{2v} = \alpha_{2e}$
	$\mu_{3v} = 0.75 \cdot \mu_{3e}$ $, \alpha_{3v} = \alpha_{3e}$

Figure 17: Finite element mesh and material parameters of the actuator. Not drawn to scale.

in circumferential direction are used for the finite element mesh. In thickness direction the elastomer is discretised by four elements. The convergency of the results is checked by h-refinement and with elements of higher polynomial order. To identify the material parameters a uniaxial pull test is analyzed, see Figure 18 on the left hand side. On the right hand side of Figure 18, the actuator described previously is considered. Both curves are fitted to the experimental results. In the load-deflection curve the displacement in z-direction of the inner edge is depicted versus the load, which is uniformly applied in

z-direction. The material parameters are qualitatively fitted to these curves and depicted in Figure 18. In this way the material parameters found are given on the right-hand side of Figure 17 for the used Ogden-material model. The bulk-modulus is defined by $\kappa = 1000\,\mu_e$ with $\mu_e = 1/2 \sum_{p=1}^{3} \alpha_{pe}\,\mu_{pe}$. Because of the lack of experimental data we assumed

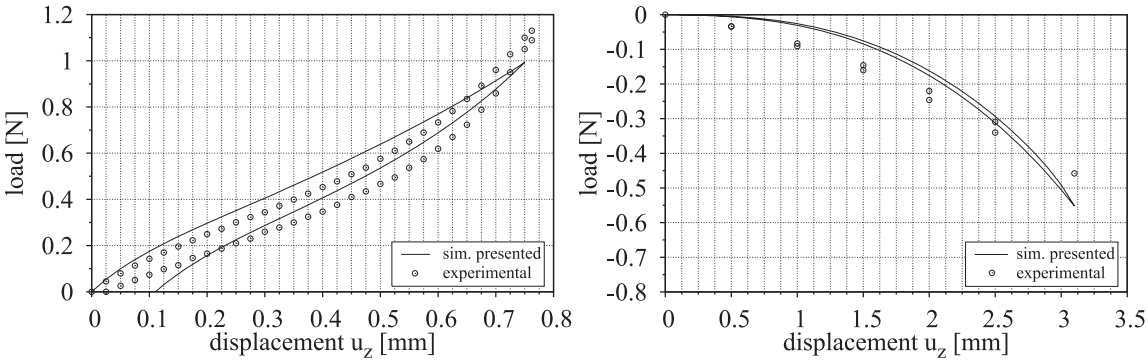

Figure 18: Uniaxial pull test of the dielectric elastomer (left) and of the considered actuator without electrodes (right) to indicate the material parameters. Experimental results are taken from [35] and [33], respectively.

the electromechanical parameters $c_1 = 1 \cdot 10^{-11}\,Fmm^{-1}$ and $c_2 = 5 \cdot 10^{-11}\,Fmm^{-1}$. Unfortunately, the loading rate is also unknown, thus we assume a viscosity of ${}^1\eta_{iso} = 10\,Ns\,mm^{-2}$. In the next step, the considered actuator is investigated for four different pre-strains, see also [34]. X First the displacement of the inner edge is prescribed with

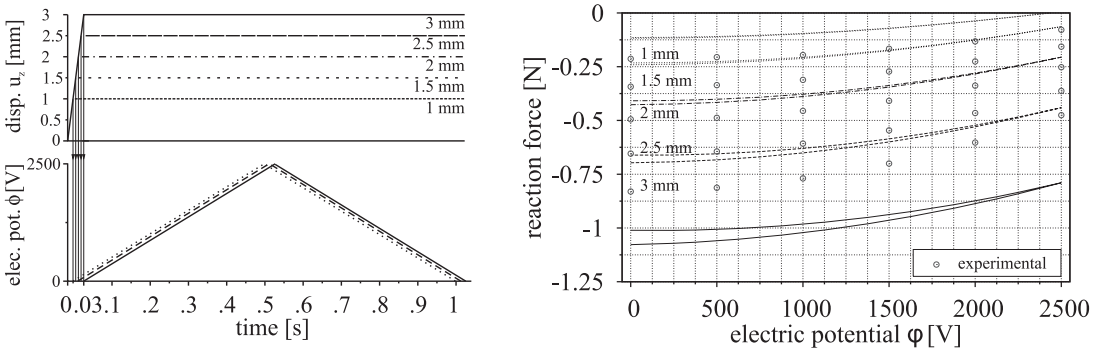

Figure 19: Loading conditions with 1–3 mm pre-strain with following electric loading (left) and results for the different pre-strains (right). Experimental results are taken from [34].

$1\,mm$ to $3\,mm$ in steps of $0.5\,mm$. Afterwards the displacement is frozen and a support in vertical direction is added. The reaction force of the support is measured, which is caused by an applied triangular-shaped electrical potential with a frequency of 1 Hz. The loading conditions are shown on the left hand side and the results on the opposite side in Figure 19. It shows also that an increase of the pre-strain results in an increase of the actuating power during an electrical loading, which qualitatively coincides with the experimental data. Furthermore the simulation shows an enlargement of the hysteresis by increasing electric field and pre-strain. This fact does not correspond to the experimental data, but by using a better choice of the viscosity parameters an improved approximation to the experimental curves should be possible.

5 Conclusion

Due to the growing interest of small but powerful electromechanical actuators, one of the aims should be reliable numerical models.
In this paper a nonlinear visco-electroelastic model for dielectric elastomers is presented. This model is based on the laws of electricity and elasticity and incorporates time dependent effects, large strains and electromechanical coupling. The deformation gradient is multiplicatively decomposed into an elastic and a viscous part. The model is embedded in a thermodynamic consistent framework, based on the definition of a free energy function for the elastic, electric and viscous parts. The irreversible viscous part serves as internal variable describing the dissipation of the material. A consistent finite element approximation is formulated employing displacements and the electric potential as independent variables. The presented examples demonstrate the efficiency of the developed formulation within various applications.
To operate with moderate electric fields, thin layers are a possible solution and are state of the art. Hence the usage of shell elements would be advantageous, to reduce numerical problems like locking effects. A further important effect is to improve the theory about anisotropic effects within the material. A strain induced effect on the change of material properties would be a good approximation for the polymeric behavior.

References

[1] Donald, J.L. *Engineering analysis of smart material systems* John-Wiley & Sons, Inc.: Hoboken, New Jersey, 2007.

[2] Janocha, H. et al. *Adaptronics and smart structures: basics, materials, design, and applications* (2nd edn). Springer-Verlag: Berlin Heidelberg, 2007.

[3] Shahinpoor, M., Schneider, H.-J. *Intelligent materials* RSC Publishing: Cambridge, 2008.

[4] Carpi, F. *Dielectric Elastomers as Electromechanical Transducers* Elsevier: Amsterdam, 2008.

[5] Kloos G. *Maxwell Stresses and Dielectric Materials* Trans Tech Publications LTD: Stafa-Zuerich, 2008.

[6] Kornbluh, R., Pelrine, R., Pei, Q., et al. *Electroelastomers: applications of dielectric elastomer transducers for actuation, generation, and smart structures* Proceedings of SPIE Smart Structures and Materials, 2002.

[7] Malvern, L.E. *Introduction to the Mechanics of a Continuous Medium* Prentic-Hall: New Jersey, 1969. *Proceedings of SPIE Smart Structures and Materials* 2002: industrial and commercial applications of smart structures technology **4698**(2002b):254–270.

[8] Bar-Cohen, Y. *Electroactive polymer (EAP) actuators as artificial muscles: reality, potential, and Challenges* SPIE Press Book, 2004.

[9] Kwang, J. K., Satoshi, T. *Electroactive Polymers for Robotic Applications* Springer-Verlag: London, 2007.

[10] Bar-Cohen, Y. Electroactive polymers as an enabling materials technology *Proceedings of the Institution of Mechanical Engineers – Part G – Journal of Aerospace Engineering* 2007; **221**(4):553–564.

[11] Brochu, P., Qibing, P. Advances in Dielectric Elastomers for Actuators and Artificial Muscles *Macromolecular Rapid Communications* 2010; **31**(1):10–36.

[12] Eringen, A.C., Maugin, G.A. *Electrodynamics of Continua I: Foundations and Solid Media* Springer-Verlag: New-York, 1990.

[13] Reese S. and Govindjee S. A theory of finite viscoelasticity and numerical aspects. *International Journal for Solids Structures* 1998; **35**(26-27):3455–3482.

[14] Reese S. and Govindjee S. A presentation and comparison of two large deformation viscoelasticity models. *Journal of Engineering Materials and Technology* 1997; **119**(3):251–255.

[15] Lubliner J. A model of rubber viscoelasticity *Mechanics Research Communications* 1985; **12**(2):93–99.

[16] Lee E.H. Elastic-plastic deformation at finite strains *Journal of Applied Mechanics* 1969; **36**(1):1–6.

[17] Lion A. A constitutive model for carbon black filled rubber: Experimental investigations and mathematical representation*Continuum Mechanics and Thermodynamics* 1996; **8**(3):153–169.

[18] Ask A., Menzel A. and Ristinmaa M. On the modelling of electro-viscoelastic response of electrostrictive polyurethane elastomers *IOP Conference Series: Materials Science and Engineering* 2010; **10**(1).

[19] Ask A., Menzel A. and Ristinmaa M. Electrostriction in electro-viscoelastic polymers *International Journal For Numerical Methods in Engineering* 2012; **50**:9–21.

[20] Ask A., Menzel A. and Ristinmaa M. Phenomenological modeling of viscous electrostrictive polymers *International Journal Of Non-Linear Mechanics* 2012; **47**(2):156–165.

[21] Coleman, B.D. and Noll, W. The thermodynamics of elastic materials with heat conduction and viscosity *ARMA* 1963; **13**(26–27):167–178.

[22] Coleman, B.D. and Gurtin, M. Thermodynamics with internal variables *Journal of Chemical Physics* 1967; **47**(597):597–613.

[23] Vu D.K., Steinmann P. and Possart G. Numerical modelling of non-linear electroelasticity *International Journal For Numerical Methods in Engineering* 2007; **70**:685–704.

[24] Vu D.K. and Steinmann P. Nonlinear electro- and magneto-elastostatics: Material and spatial settings *International Journal of Solids and Structures* 2007; **44**:7891–7905.

[25] Vu D.K. and Steinmann P. Material and Spatial Motion Problems in Nonlinear Electro- and Magneto-elastostatics *Mathematics and Mechanics of Solids* 2010; **15**(2):239–257.

[26] Pao YH. Electromagnetic Forces in Deformable Continua *Mechanics Today* 1978; **4**:209–305.

[27] Eringen A.C. On the foundations of electroelastostatic *International Journal of Engineering Science* 1963; **1**:127–153.

[28] Dorfmann A. and Ogden R.W. Nonlinear electroelasticity *Acta Mechanica* 2005; **174**(3–4):167–183.

[29] Bustamente R. and Ogden R.W. Universal relations for nonlinear electroelastic solids *Acta Mechanica* 2006; **182**(1–2):125–140.

[30] Bustamante R., Dorfmann A. and Ogden R.W. Nonlinear electroelastostatics: a variational framework *Zeitschrift fuer Angewandte Methematik und Physik* 2009; **60**:(1)154–177.

[31] Bustamante R., Dorfmann A. and Ogden R.W. On electric body forces and Maxwell stresses in nonlinearly electroelastic solids *International Journal of Engineering Science* 2009; **47**(11–12):1131–1141.

[32] Mc Meeking R.M. and Landis C.M. Electrostatic Forces and Stored Energy in Deformable Dielectric Materials *Journal of Applied Mechanics* 2005; **72**(4):581–590.

[33] Deodhar A., York A., Hodgins M. and Seelecke S. Finite Element modeling of electromechanical behavior of a dielectric Electroactive Polymer Actuator *Prodedings of SPIE* 2011; **7978**(1–2):125–140.

[34] York A. and Dunn J. and Seelecke S. Experimental characterization of the hysteretic and rate-dependent electromechanical behavior of dielectric electro-active polymer actuators*Smart Materials and Structures* 2010; **19**(1–2):125–140.

[35] Deodhar A. Electromechanically coupled finite element model of a circular electroactive actuator *Master Thesis, North Carolina State University,* 2011;

[36] Miehe C. and Rosato D. A rate-dependent incremental variational formulation of ferroelectricity *International Journal of Engineering Science* 2011; **49**(6):466–496.

[37] Miehe C. and Rosato D. and Kiefer B. Variational principles in dissipative electromagneto-mechanics: A framework for the macro-modeling of functional materials *International Journal for Numerical Methods in Engineering* 2011; **86**(10):1225–1276.

[38] Maple (12.0). Maplesoft, a division of Waterloo Maple Inc., Waterloo, Ontario.